Improvements in Simulating a Mach 0.80 Transonic Truss-Braced Wing Configuration using the Spalart-Allmaras and k-ω SST Turbulence Models

Daniel Maldonado*, Jeffrey A. Housman†, Michael G. H. Piotrowski‡, Cetin C. Kiris §
NASA Ames Research Center, Moffett Field, CA, 94035, USA

Craig A. Hunter¶, Sally A. Viken**, S. Naomi McMillin††, William E. Milholen‡‡
NASA Langley Research Center, Hampton, VA, 23681, USA

Teams from the NASA Ames Research Centers (ARC) and Langley Research Center (LaRC) have been working on validating their computational fluid dynamics (CFD) results for the Boeing Mach 0.80 Transonic Truss-Braced Wing (TTBW) configuration. Experimental data used for the validation were gathered from a test conducted of a 4.5% scale Mach 0.80 TTBW model in the NASA Ames Research Center 11- by 11-Foot Transonic Wind Tunnel. The CFD simulations were initially run with both LAVA and USM3D Mixed Element solvers utilizing the Spalart-Allmaras (SA) turbulence model. A discrepancy was observed between CFD and experimental loads and moments ranging on average from 0.047 to 0.063 for lift coefficient, 16.5 to 27 in drag counts, and -0.02 to -0.032 for pitching moment, varying with the solver used. With introducing the refactored version of LAVA these values dropped to 0.034 to 0.047 for lift coefficient, 7.74 to 16.5 in drag counts, and lastly -0.012 to -0.02 for pitching moment. Based on findings from Boeing, who observed an improved comparison to experimental data when using the k-ω Shear Stress Transport (SST) turbulence model, the NASA teams conducted simulations with SST to investigate turbulence modeling sensitivities. OVERFLOW and USM3D V6 solvers were used for the comparison of SST and SA simulations. CFD results using the SST turbulence model demonstrate an improvement in matching with experimental C_L values, reducing the discrepancies seen by 0.021-0.055 (62-93% reduction in discrepancy respective to the OVERFLOW and USM3D V6). The SST model has varying effects on C_D, based on the solver / grid paradigm; for USM3D this prediction is only improved at higher angles of attack (above the cruise design point) resulting in a reduced discrepancy of 8.8 – 25 drag counts However, at the mid-to-low angles of attack, SST increases the C_D discrepancy by 4-55 counts, increasing at lower angles of attack. For OVERFLOW this discrepancy only exists at the low angles of attack and maxes out at 10 counts of drag. Above $\alpha = 1.5^\circ$ OVERFLOW SST reduces discrepancy by 9.3 drag counts on average.

I. Nomenclature

C_D	=	drag coefficient
C_L	=	lift coefficient
C_{My}	=	pitching moment coefficient
C_p	=	pressure coefficient
k	=	turbulent kinetic energy
M	=	Mach number
N	=	number of grid cells or nodes; degrees of freedom
Re	=	unit Reynolds number, per unit length

* Fluid Mechanics, Computational Aerosciences Branch, AIAA Member, daniel.maldonado@nasa.gov.
† Fluid Mechanics, Computational Aerosciences Branch, AIAA Senior Member, jeffrey.a.housman@nasa.gov.
‡ Computational Aerosciences Branch, AIAA Student Member, michael.g.piotrowski@nasa.gov.
§ Computational Aerosciences Branch Chief, Computational Aerosciences Branch, AIAA Senior Member, cetin.c.kiris@nasa.gov
¶ Configuration Aerodynamics Branch, craig.hunter@nasa.gov
** Configuration Aerodynamics Branch, AIAA Associate Fellow, s.a.viken@nasa.gov
†† Configuration Aerodynamics Branch, AIAA Senior Member, susan.n.mcmillin@nasa.gov
‡‡ Configuration Aerodynamics Branch, AIAA Senior Member, william.e.milholen@nasa.gov

T_u	=	turbulence intensity, percentage
y^+	=	dimensionless distance from the wall measured in viscous units
α	=	angle of attack, degrees
ß	=	angle of sideslip, degrees
η	=	spanwise position nondimensionalized by wing semispan
μ	=	laminar viscosity
μ_t	=	turbulent viscosity
μ_t/μ	=	turbulent viscosity ratio
∞	=	freestream condition

II. Introduction

The Boeing Transonic Truss-Braced Wing (TTBW) originated from a NASA/Boeing Subsonic Ultra-Green Aircraft Research (SUGAR) effort to develop advanced subsonic transport concepts and technologies that meet or exceed NASA-defined system-level metrics of reduced noise emission, nitrogen oxides emission, and energy/fuel consumption. The initial concept of the Transonic Truss-Braced Wing, the TTBW SUGAR High vehicle, was identified as a technology with promising fuel burn reduction capabilities [1]. The concept featured a high aspect-aspect-ratio (AR ~ 19.55) strut- and truss-braced high wing designed for a high lift-to-drag ratio (L/D) [2]. The high aspect ratio of the wing (100% greater than the baseline cantilever wing vehicle) reduces induced drag. The high wing provides the opportunity for the integration of larger bypass ratio engines. Together, these benefits contribute to decreased fuel consumption. The TTBW concept has evolved through four phases of research; phases III and IV investigated the Mach 0.745 and Mach 0.80 variants of the TTBW, along with their respective wind tunnel tests, in order to assess the performance of the vehicles and gather data for validation [3,4].

Since 2017, NASA Ames Research Center (ARC) and Langley Research Centers (LaRC) have been working on developing best practices for the computational analysis of the Boeing TTBW aircraft. This has been achieved through grid convergence studies, code-to-code comparisons, and validation with experimental data [5,6]. The aim remains to improve CFD performance predictions for this kind of vehicle where the truss interference effects are not well understood.

The NASA codes used for these previous studies were LAVA and USM3D. Initial analysis was performed using the Spalart-Allmaras (SA) one-equation turbulence model, which was already implemented in both of the solvers. Further developments to the codes, such as the refactoring of LAVA and the introduction of mixed elements to USM3D, have shown massive improvements in terms of comparison with experimental data, convergence, and turnaround time.

In the Phase IV report of the TTBW BAART contract, Boeing compared their CFD results using OVERFLOW with both the SA and the two-equation k-ω Shear Stress Transport (SST) [7] turbulence models against data obtained from testing a 4.5% scale model of the Mach 0.745 configuration in the NASA Ames Research Center (ARC) Unitary Plan 11-Foot Transonic Wind Tunnel (11-Ft TWT) [4,8]. The comparison showed that the SST turbulence model resulted in a better match to experimental data, in terms of C_L and C_{My},. Relative to the SA turbulence model, SST simulations resulted in a positive angle of attack shift in the C_L-α curve, effectively lowering the C_L values at each angle of attack. In terms of the drag polar, the SA turbulence model results had better agreement with experimental data at lift coefficients near and below the design C_L of 0.695. The SST turbulence model had better agreement at the higher lift coefficients [8].

This paper discusses the latest efforts to narrow the gap between CFD and experimental results obtained from a high-speed performance test on a 4.5% scale model of the Mach 0.80 TTBW configuration in the NASA ARC 11-Ft TWT. The efforts consist of improvements to the LAVA and USM3D solvers, as well as expanding the use of turbulence models to include SST. At the time of this paper, LAVA did not have SST implemented; therefore, with the interest of continuing to use at least two solvers for code-to-code comparison, a third NASA CFD flow solver, OVERFLOW, is used to obtain the SST results for the structured overset grids.

III. Computational Fluid Dynamics Solvers

A. LAVA

The Launch, Ascent, and Vehicle Aerodynamics (LAVA) framework [9] contains CFD flow solvers developed with the intent of simulating complex geometry and flow-fields, using flexible meshing options. The framework supports Cartesian, structured overset, and unstructured arbitrary polyhedral mesh paradigms. In this study, the

structured overset grid methodology is applied, in which overlapping, body-fitted meshes are constructed on the geometry to serve as the computational domain.

The compressible Reynolds-averaged Navier-Stokes (RANS) equations are solved using a finite-difference formulation applied to the nonorthogonal curvilinear transformed system of equations in strong conservation law form [10]. The SA turbulence model [11] with Rotation/Curvature Correction [12] and Quadratic Constitutive Relationship (SARC-QCR2000)[13] is used to close the Reynolds-averaged system. The SARC-QCR2000 model will be referred to as SA-RC-QCR in this paper. In the current work, a second-order accurate convective flux discretization is used for the mean-flow equations, consisting of a modified Roe scheme [14,15] with third-order left/right state reconstruction and a Koren limiter. The turbulence model convective terms are discretized using first-order upwinding.

The production version of LAVA used for the previous TTBW studies has been refactored to accelerate performance. The numerics for the right hand side (RHS) are the same, while the viscous stress in the loads calculation is now 2nd order. The turbulence model equation is solved segregated from the mean-flow equations. The linear solver uses an incomplete lower-upper factorization with level 0 fill (ILU(0)) to precondition the Krylov-subspace linear solver generalized minimal residual method (GMRES) [16]. The refactored solver is hybrid Message Passing Interface (MPI)/OpenMP and all of the RHS routines have been vectorized. Local pseudotime stepping is used to accelerate convergence with a self-ramping pseudotime CFL starting at 5 and ramping up to 5000. Tiling of the computational zones is used for an on-the-fly domain decomposition in order to enable a scalable cache-friendly parallel algorithm. Best practice simulations of the TTBW for the SA turbulence model are now run using the refactored LAVA solver. LAVA solutions throughout the paper will be referred to as either LAVA SA-RC-QCR or LAVA SA.

Performance Improvements with Refactorization of the Code

The refactorization of the code has improved the accuracy of the solution and convergence rate to steady-state while lowering the resource cost and turnaround time by reducing pre-processing, post-processing, and CFD run time. The accuracy of the solver has primarily improved due to the use of 2nd order accurate viscous stress terms in load calculations, since the RHS evaluation is identical to the previous version of the solver. This is supplemented by the improved convergence due to the strong linear solver. The solver has also simplified pre-and post-processing by removing the need to physically partition the domain for parallel simulations; this provides the ability to adapt the number of cores used for a simulation based on available resources resulting in faster turnaround times. Additionally, the domain connectivity routine for overset meshes has been improved, decreasing the processing time from 8 hours to approximately 5 minutes. Overall, the refactored solver has shown varying speed-ups in solution convergence ranging from 1.5 – 31.7x, depending on the case. For free air simulations, such as those discussed in this study, a 1.5-4.0x speedup has been observed when comparing against CFL-accelerated solutions from the production solver. While this method was the best practice for TTBW simulations, the general best practice for the production solver is to use a lower, more robust CFL. In most TTBW cases that required this lower CFL, an 8-16x speedup was seen when using the refactored LAVA solver. For the more complex TTBW simulations in which the wind tunnel was included in the simulation, there was a 12-27x reduction in SBU cost, depending on the desired test section flow condition set by the tunnel outflow boundary condition. Additionally, the refactored LAVA simulations attenuated oscillatory behavior of the test section Mach number, decreasing the standard deviation of this quantity by nearly 40x. Performance improvement from this study are presented in Table 1. Figure 1 demonstrates how refactored LAVA compares better with experimental results. Figures 1 e-f compare C_p profile data at both a specific angle of attack and its corresponding experimental C_L value. Both demonstrate improved comparisons with the refactored solver, particularly in predicting the shock location. All of these solutions were ran using SA-RC-QCR. For the remainder of the paper LAVA will refer to the refactored version of LAVA.

Table 1. Performance Improvement using Refactored LAVA for free air simulations.

	CPUs	Walltime	C_L Standard Deviation	C_D Standard Deviation	C_{My} Standard Deviation	Flow Residual Reduction	Turbulent Residual Reduction
Production	840	287 min	2.0e-6	3e-7	3.0e-6	7.9e-6	1.1e-4
Refactored	840	100 min	2.0e-7	1.3e-7	7.4e-7	3e-6	3.1e-6
Improvement	1	2.9x	10x	2.3x	3.3x	2.6x	35x

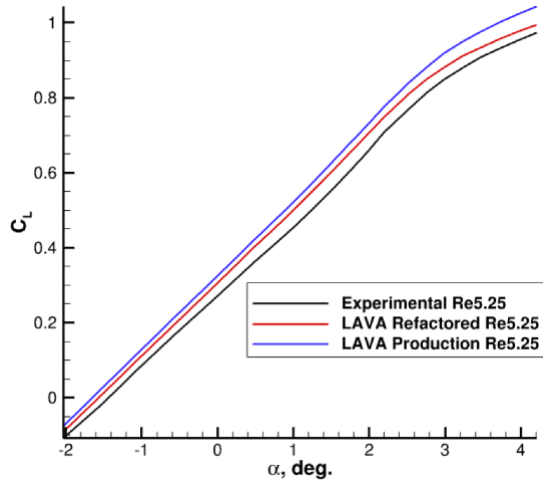

a. C_L - α Curve

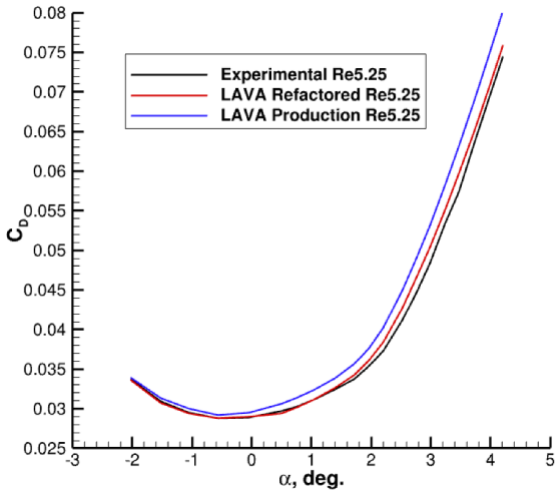

b. C_D - α Curve

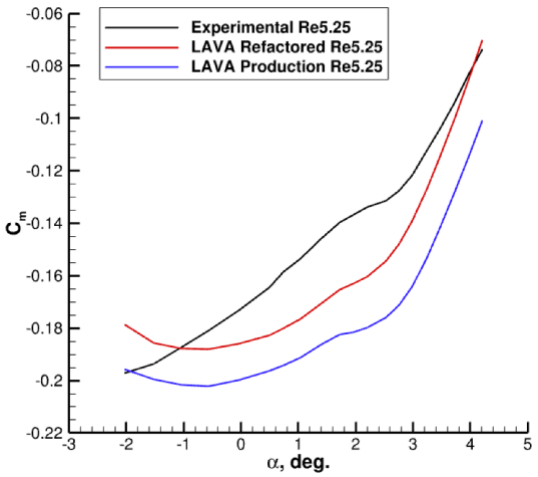

c. C_{My} - α Curve

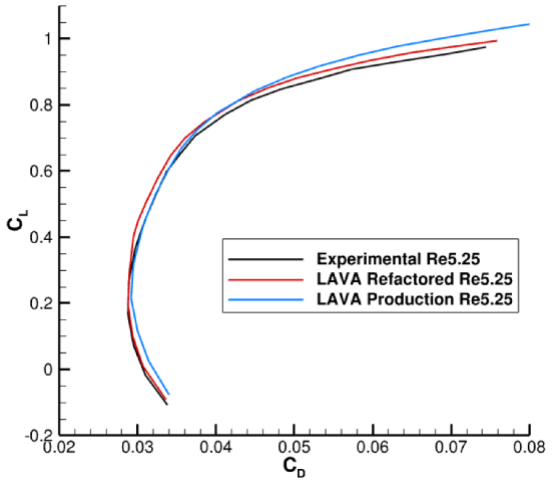

d. Drag Polar

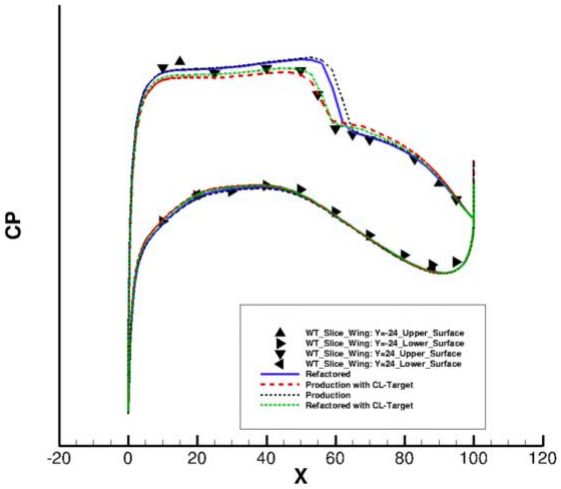

e. C_p Profile Comparison at 24% Span, α = 2.198

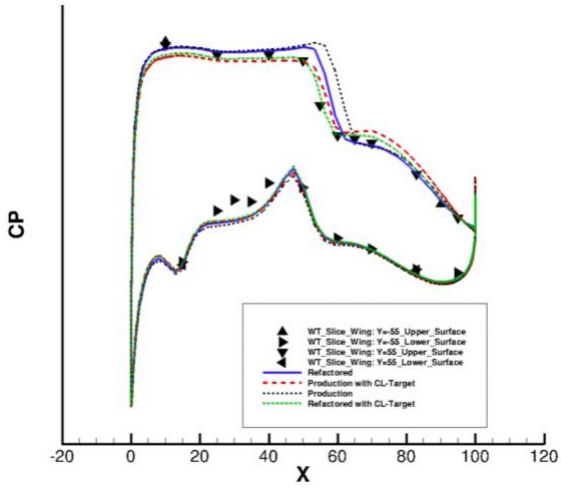

f. C_p Profile Comparison at 55% Span, α = 2.198

Fig. 1 Angle of attack sweep and pressure coefficient profiles generated using production and refactored LAVA compared with experiment for the WT WBSNFV configuration at M_∞ = 0.80, *Re* = 5.25 x 10^6/ft.

B. OVERFLOW

Due to the fact that the SST model was still in development for LAVA at the time of this paper, the team decided to use OVERFLOW version 2.2n [17] in order to obtain SST results on the same structured overset grid used for LAVA simulations. OVERFLOW simulations were conducted using both SA and SST turbulence models in order to isolate the differences resulting from the turbulence model. Additionally, a comparison of the LAVA SA and OVERFLOW SA solutions are used to understand differences due to solver strategies. OVERFLOW is an implicit Navier-Stokes code developed as a structured overset grid system flow solver with two operational modes, OVERFLOW and OVERFLOW-D. OVERFLOW-D-mode is used to properly connect the grid system by blanking mesh points that lie inside of the geometry and removing excess overlap between adjacent grids. To maintain the connectivity used with the LAVA simulations, the OVERFLOW-mode of the solver was run using the blanked grid file and the XINTOUT file generated during LAVA connectivity. XINTOUT provides the interpolation and blanking information required by the flow solver to connect multiple grids.

For SA simulations, the SA-neg-noft2 with RC-QCR2000 was used with one turbulence model iteration per flow solver iteration and no compressibility correction. The left-hand side (LHS) approximations were made with ADI Factorization (ARC3D Beam-Warming Block Tridiagonal scheme). Initial simulations were conducted using central differencing for the right hand side; however, this was showing instabilities which led to changing to a 2nd order spatial differencing upwind Roe scheme with the Koren limiter. A first-order convective flux discretization was used for both turbulence models. All other inputs were set to default values.

For the SST simulations, the SST-2003 model [18] with RC-QCR2000 [19] and DDADI LHS was used with five turbulence model iterations per flow solver iteration. Initially, simulations were attempted with one turbulence model step per flow iteration; however, this was increased to maintain a stable solution. The CFLT, used to evolve the turbulence model equation, was reduced to 0.1. All the remaining settings were consistent with the SA setup. Even though both OVERFLOW SA and SST are run with RC-QCR, they will at times be referred to as OVERFLOW SA and OVERFLOW SST to simplify notation.

C. USM3D

USM3D is a cell-centered, finite-volume, Reynolds-averaged Navier-Stokes (RANS) flow solver that is part of the TetrUSS (Tetrahedral Unstructured Software System) package [20-22] developed at NASA Langley Research Center (LaRC). The legacy USM3D production code [20,21] utilizes an unstructured tetrahedral (tet) mesh, and fully turbulent solutions were computed with the standard SA turbulence model. A more recent version of USM3D, which can handle mixed element grids [19], was also utilized due to its improvements to robustness and speed. This "Mixed Element USM3D" solver uses a new solution methodology known as Hierarchical Adaptive Nonlinear Iteration Method (HANIM). HANIM is a strong nonlinear solver that improves the robustness, efficiency, and automation of RANS solutions. HANIM makes use of a matrix-free linear solver for the exact linearization of RANS equations and a nonlinear control method for solution update. Together, these enhance the iterative scheme with a mechanism for automatic adaption of the operational pseudo time step, to increase convergence rates and overcome transitional instabilities and limit cycles. Further enhancements come from a line-implicit preconditioner that simultaneously updates a preconditioned solution at all cells of a grid line based on local grid connectivity. Mixed Element USM3D has been parallelized in a fashion that maximizes CFD solution throughput, with careful and efficient inter-partition communication. This results in excellent scalability across the full range of grid partition size and number of partitions. Mixed element meshes have prismatic cells in the boundary layer, tetrahedral cells in the outer grid, and pyramidal cells in the transition between the two regions. The current best practice for fully turbulent TTBW solutions is to use the SA turbulence model with the mean stress-strain Quadratic Constitutive Relationship (SA-QCR2000). The SA-QCR2000 model will be referred to as SA-QCR in this paper. For the comparison between SA and SST, the legacy USM3D production solver is used and is referred through paper as USM3D V6. In this paper the Mixed Element USM3D solutions will be referred to as USM3D Mixed Element.

Performance Improvements with USM3D Mixed Element

The USM3D Mixed Element has demonstrated reductions in time to solution by 70x on benchmark 3D RANS problems, and 5X-20x on complex real-world aerodynamics simulations. For the TTBW cases analyzed in this study, Mixed Element USM3D demonstrated reductions in time to solution of 7-10x compared to the legacy USM3D flow solver. Lastly, grid refinement studies show that the Mixed Element solutions are less sensitive to the grid size. This and more comparisons between the two versions of the USM3D solver can be found in the Mach 0.8 NASA Technical Memorandum [6].

IV. Mach 0.80 Wind Tunnel Test

A. Wind Tunnel Test Setup

The Mach 0.80 TTBW high-speed wind tunnel test was conducted at the NASA Ames Research Center 11- by 11-Foot (11-Ft) Transonic Wind Tunnel (TWT) Facility. The TTBW model tested was a full span, 4.5% scale representation of the high-speed TTBW design configuration (1104-001-RG) and the reference parameters for this model are shown in Table 2. The experimental data corresponding to this study were acquired during the Mach 0.80 TTBW Test 367 Run 378. This run consists of angles of attack ranging from $\alpha \approx -2.04°$ to $\alpha \approx 4.26°$ with no sideslip, a freestream Mach of 0.80, and Re = 5.25 x10^6/ft. The conditions from this run are provided in Table 3. The wind tunnel (WT) configuration investigated is composed of the wing and wing fairing, fuselage body and sponson, wing-supporting strut, nacelle and pylon, flap hinge fairings, and vertical tail, referenced as WBSNFV. The wind tunnel configuration includes a modification of the aft portion of the fuselage and vertical tail to include a cavity that allowed the mounting of the test article to the support system (sting). The 4.5% scale model of the full configuration is shown installed in the wind tunnel in Fig. 2.

Table 2. Reference parameters for the 4.5% scale Mach 0.80 TTBW model.

4.5% Model Scale Reference Parameters	
Reference Area	430.7256 in^2
Reference Chord	4.963 in
Span Length	91.769 in
Aspect Ratio	19.55

Table 3. Summary of configuration investigated and test conditions.

Configuration	M_∞	Unit Reynolds Number (x 10^6/ft)	Static Temperature (°R)
WT WBSNFV	0.80	5.25	480.78

(a) Front oblique view. (b) View from under side of model.

Fig. 2 4.5% scale, Mach 0.80 TTBW model, installed in the NASA ARC 11-Ft TWT.

B. Data Acquisition

Forces and moments were computed with cavity, buoyancy, and wall corrections using the Transonic Wall Interference Correction System (TWICS) [23,24]. Surface static pressures were gathered using 144 pressure taps placed along the chordwise direction at 14 wingspan locations and 82 pressure taps along 6 strut spanwise locations. The pressure taps were placed on the upper surface of the right strut and wing and on the lower surfaces of the strut and wing [23].

V. Grid Refinement Study

In order to determine that a sufficiently refined grid is used, a grid refinement study was performed. Three flight scale grid levels were used for OVERFLOW and four for USM3D simulations. These grids were previously generated and used for a grid refinement study involving LAVA and USM3D V6 SA solutions. The corresponding data, as well as a detailed process of the generation of these grids, are available in the *Comparison of Computational Predictions of the Mach 0.80 Transonic Truss-Braced Wing Configuration with Experimental Data* [6].

A. Grid Convergence Plots

When examining grid refinement data, the loads were plotted against a function with a representation of the cell size and the expected order of convergence of the solver, *p*. For these simulations, the order of numerical accuracy is approximately 2 and the cell size is represented by $N^{-1/3}$ where N is the number of nodes or cells depending on the grid paradigm. The final independent variable used for the relationship incorporates the order of convergence into the size representation resulting in $N^{-2/3}$. Plotting this value versus the loads of the corresponding grids will, in an ideal scenario, produce a linear fit of the data in the asymptotic regime. In reality this might not be a linear fit because the order of convergence can vary with coarser grids as well as with the presence of shocks and geometric singularities. Additionally, data might not have monotonic behavior due to unresolved small-scale or unsteady flow artifacts being picked up with finer grids.

B. SA vs SST Grid Refinement Results

A grid refinement study was conducted with both USM3D V6 and OVERFLOW solvers comparing the SA and SST turbulence models. This was done to confirm that the grids were sufficiently refined and to better understand the grid convergence behavior of the turbulence models. Grid refinement study results are plotted in Figure 3. For the overset grids run with OVERFLOW, a grid is considered sufficiently refined if the drag values are within 10 drag counts of the asymptotic value. We can apply a similar criterion to the USM3D grids. Tables 4 and 5 show grid information, loads, and asymptotic values for the SA vs SST grid refinement study for the USM3D V6 and OVERFLOW solvers, respectively.

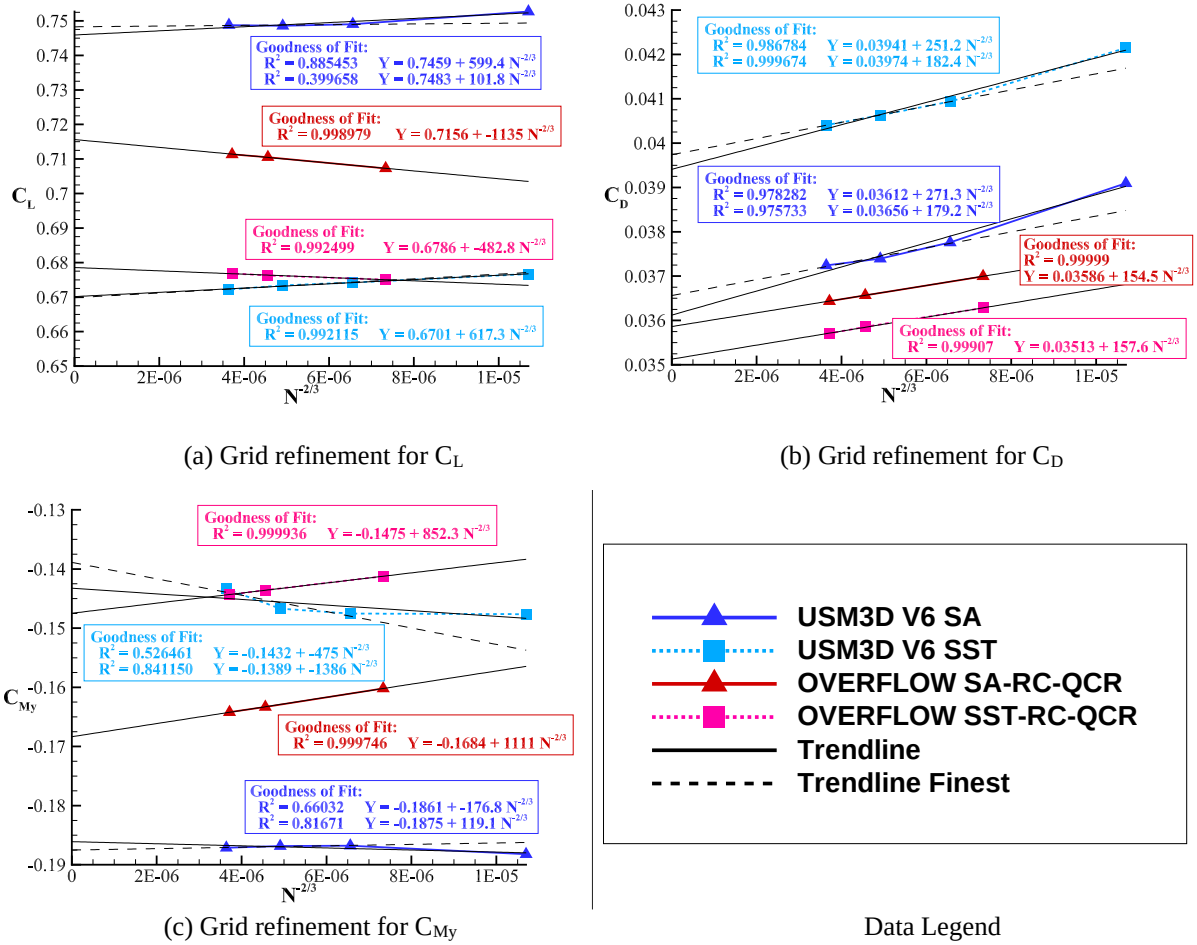

(a) Grid refinement for C_L

(b) Grid refinement for C_D

(c) Grid refinement for C_{My}

Data Legend

Fig 3. Grid refinement study comparing SA and SST turbulence models for USM3D V6 and OVERFLOW.

Table 4. USM3D V6 SA vs SST Grid Refinement Study Results at M=0.8, Re=5.25 x10^6/ft, and α = 2.0

		SA			*SST*		
Grid Levels	***Cells***	C_L	C_D	C_{My}	C_L	C_D	C_{My}
Coarse	28,405,714	0.7526	0.03909	-0.1882	0.67669	0.04215	-0.1476
Medium	59,462,979	0.7490	0.03775	-0.1868	0.67421	0.04094	-0.1475
Fine	92,025,695	0.7485	0.03739	-0.1868	0.67338	0.04063	-0.1467
Extra Fine	144,022,412	0.7487	0.03724	-0.1871	0.67219	0.04041	-0.1434
Asymptotic All 4	∞	0.7459	0.03612	-0.1861	0.6701	0.03941	-0.1432
Asymptotic Top 3	∞	0.7483	0.03656	-0.1875	0.6698	0.03974	-0.1389
Slope		101.8	179.2	119.1	617.3	182.4	-1386

Table 5. OVERFLOW SA vs SST Grid Refinement Study Results at M=0.8, Re=5.25 x10^6/ft, and α = 2.0.

		SA			*SST*		
Grid Levels	***Vertices***	C_L	C_D	C_{My}	C_L	C_D	C_{My}
Medium	50,342,233	0.7073	0.03700	-0.1602	0.6750	0.03628	-0.1412
Fine	102,726,324	0.7105	0.03657	-0.1633	0.6763	0.03586	-0.1436
Extra Fine	139,766,019	0.7113	0.03644	-0.1642	0.6768	0.03571	-0.1443
Asymptotic	∞	0.7156	0.03586	-0.1684	0.6786	0.03513	-0.1475
Slope		-1135	154.5	1111	-482.8	157.6	852.3

With respect to C_L, a large difference is apparent between USM3D V6 SA and OVERFLOW SA. This is not the case when comparing the SST turbulence model results. In terms of sensitivity, it appears that the USM3D V6 SA solutions converge at a much quicker rate relative to grid resolution. Once at the medium grid there is not much change in loads with added refinement just oscillations about a particular load. For this reason, an additional asymptotic value was computed using only the finest 3 grids. Due to the oscillation of the loads the linear fit is poor, but the value is essentially converged. Surprisingly, the OVERFLOW SA solution has much more sensitivity to grid resolution than the USM3D V6 SA results, approximately 10 times more. However, all the grids still fall in the asymptotic regime which can be seen by the linear fit of the data. Moving onto the SST results, we see an opposite behavior between the two solvers. The OVERFLOW SST solutions appears less dependent on grid size than the SA solution while the USM3D V6 SST loads change more as the grid is refined than USM3D V6 SA cases.

Moving on to the drag plots, for OVERFLOW the fine grid for both the SA and SST fall within 10 drag counts of the asymptotic value and is considered to be sufficiently fine for the simulation. For USM3D, similar results are seen as with the USM3D V6 SA C_L data; as the grids get finer the slope between data points get flatter. Analyzing the USM3D C_D values using the overset convergence criterion we see that the medium grid falls within 12 drag counts of the asymptotic value. Due to how these values are changing leveling out as the grid is refined, it is likely that drag value as $N^{-2/3}$ approaches zero will be higher than the current asymptotic value, lowering that drag count difference. Additionally, using the medium grid will allow a better comparison with previously solutions, as they also used the medium grid level. The sensitivity of C_D relative to grid size is consistent between both solvers and both turbulence models. One thing to note is that while the drag increases with increased refinement for the USM3D V6 SST results, it decreases in the OVERFLOW SST solutions. This will be discussed with the angle of attack sweep data.

For pitching moment, we see similar behavior as that seen in the C_L grid refinement study. The SA and SST models cluster closer together for the OVERFLOW simulations while appearing to be more sensitive to grid size. With USM3D V6 SA solutions there is not much change in the pitching moment after the medium grid. For the SST model however, the extra fine grid shows a sharp decrease in pitching moment. An extra grid level would need to be generated to better understand the trend of this pitching moment. However, since most the other loads are moving towards convergence this extra investigation will not be undertaken and the medium grid will be used for the remainder of this study.

VI. Developing Best Practices for k-ω SST

Due to the difference in implementation of the k- ω SST turbulence model in each of the solvers and how the turbulent quantities are non-dimensionalized, the values of non-dimensional turbulent kinetic energy, k, and specific rate of dissipation, ω, will differ between solvers. For this reason, the solutions will be initialized with a target eddy

viscosity ratio μ_t/μ where μ_t is turbulent viscosity and μ is laminar viscosity, as well as turbulent intensity in percentage, T_u.

A. Preliminary Simulations

Both solvers struggled to achieve a stable solution during initial test runs with the SST turbulence model. For OVERFLOW, the turbulence flow parameters were initialized with the default options; an eddy viscosity ratio of 0.1 and a turbulence intensity of 0.08165%. Additional viscous and turbulence modeling inputs were set to have 3rd order differencing for turbulent convective terms. This solution ended up diverging with problems originating around the pylon. Ultimately this was resolved by lowering the differencing for turbulent convective terms to 1st order, setting the turbulent CFL to be a factor of 10 lower than the flow CFL, and increasing the number of turbulence model iterations per flow solver iteration from 1 to 5.

During the first test cases for USM3D V6 with the SST turbulence model, it was discovered that in order to get a well-behaved solution the turbulence intensity needed to be reduced to a relatively small value. A turbulence intensity of 0.001224% was chosen. A sensitivity study was conducted by increasing and decreasing the turbulence intensity by an order of magnitude, while the eddy viscosity ratio was fixed at 0.009. Neither the USM3D nor OVERFLOW solvers experienced significant changes in the loads. For OVERFLOW solutions, the default SST initialization parameters were also included in the comparison. Even with these conditions, the loads varied by less than 0.1% at all angles of attack with the exception of the highest angle of attack, in which the pitching moment varied by 0.2% and there was a difference of 0.6 drag counts. Afterwards, an additional turbulence intensity of 0.1224% was tested and while the OVERFLOW solution had negligible changes, the USM3D solutions experienced a 50% drop in lift while producing similar drag. A turbulence intensity of 0.001224% was used to initialize the remainder of the SST results presented in the current work with an eddy viscosity ratio of 0.009.

At higher angles of attack there were noticeable oscillations in the loads. When this occurs it strongly suggests that local time stepping with RANS is inducing temporal instability as large cells and small cells run out of phase. For the cases where these oscillations were present, an extra 20K iterations were run using unsteady RANS (URANS). By transitioning to URANS with a uniform timestep for all cells, the cells can sync up and the solution locks in on a single value.

VII. Results

In order to gain a better understanding of the capabilities of the SA and SST turbulence models have in predicting the aerodynamic performance of the Mach 0.80 TTBW configuration, an angle of attack sweep corresponding to existing experimental data was conducted. The LAVA and USM3D Mixed Element SA solutions are compared with SA solutions from OVERFLOW and USM3D V6, while SA and SST solutions are compared using OVERFLOW and USM3D V6.

A. Angle of Attack Sweep

This angle of attack sweep is run on flight scale grids at M = 0.8 and Re = 5.25 x 10^6/ft. For the OVERFLOW and LAVA solutions the same structured overset grids are used. For the USM3D V6 solutions an unstructured tetrahedral grid is used, while a mixed element grid is used for the USM3D Mixed Element solver. Figure 4 plots this data and separates the structured overset grid and the unstructured grid results to more clearly compare the data.

The C_L-α curve demonstrates both sets of SST solutions show a decrease in C_L, closing the gap between CFD and experiment. However, above the angle of attack of approximately 3°, the SST begins to underpredict lift. Even with this underprediction, the difference from the experimental lift at the max angle of attack for the SST solution is still less than or equal to the corresponding difference resulting from the SA solution. The OVERFLOW and LAVA SA solutions are essentially on top of each other. The largest differences, which exist at the higher angles of attack, are still less than 0.5%. For the unstructured grids, the USM3D Mixed Element solver does predict lower C_L than USM3D V6. This difference increases with increasing angle of attack.

Looking at the C_D-α curve for the overset grids the same pattern appears where the SA solutions from OVERFLOW and LAVA are essentially predicting the same loads with differences on average of 0.4%. Comparing with experimental data, these SA solutions agree with experimental data well with an average drag count difference of 1 and less than 1% error at angles below 1.5°. After this angle of attack, the error rises up and peaks at 25 drag counts or 5%. The SST has an effect on the drag curve that essentially pivots the data slightly about 0° in a clockwise manner. This results in the SST turbulence model predicting C_D more accurately above the same 1.5° angle of attack. However, it also causes a mismatch at the lower angles of attack where it overpredicts C_D by up to 10 drag counts.

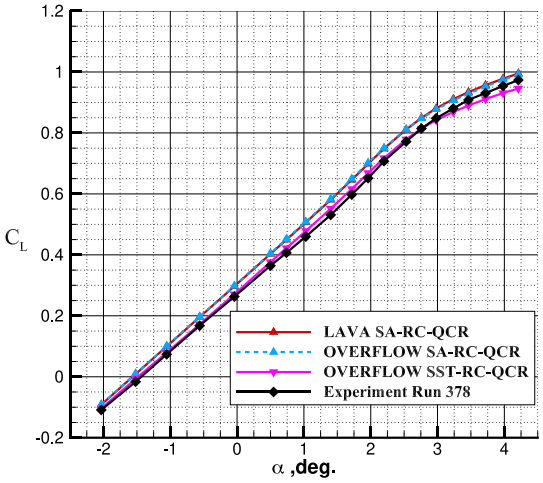

(a) C_L-α curve comparing overset grid solutions

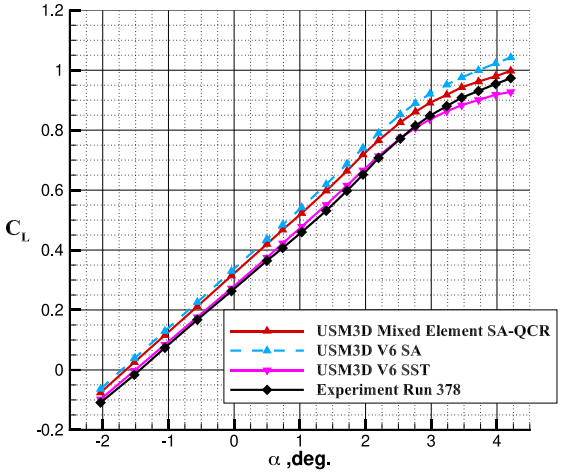

(b) C_L-α curve comparing unstructured grid solutions

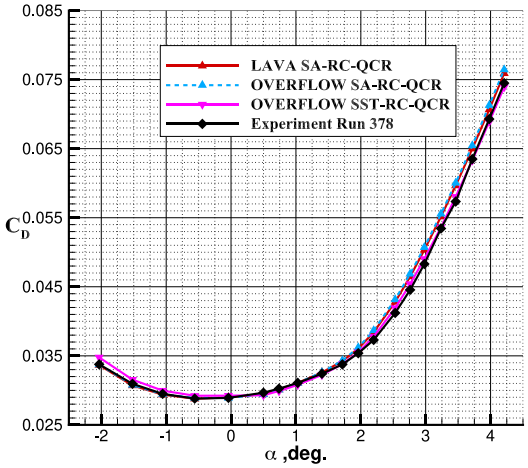

(c) C_D-α curve comparing overset grid solutions

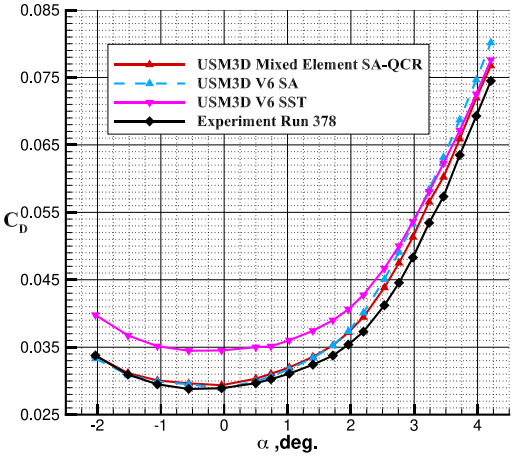

(d) C_D-α curve comparing unstructured grid solutions

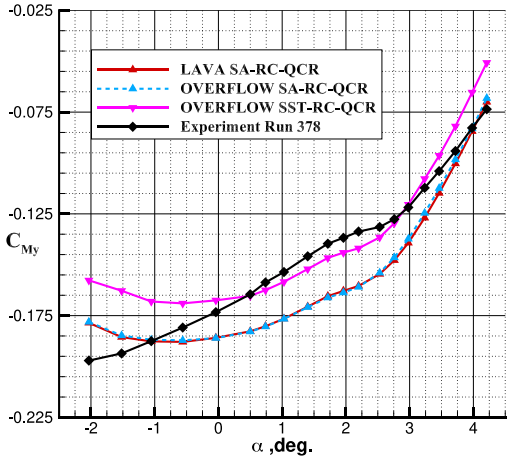

(e) C_{My}-α curve comparing overset grid solutions

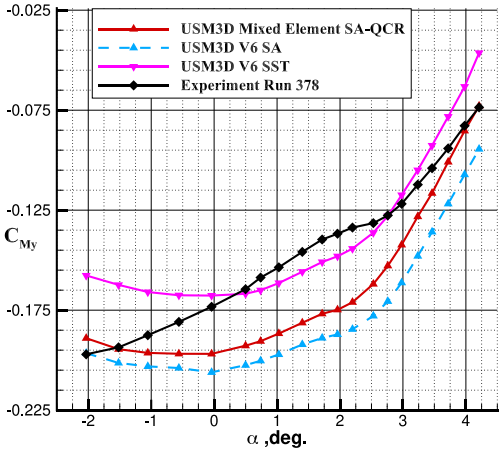

(f) C_{My}-α curve comparing unstructured grid solutions

Fig 4. Angle of Attack Sweep at Mach 0.8 and Re = 5.25 x 10^6 / ft comparing the SA and SST turbulence models for OVERFLOW and USM3D as well as comparing those results with the best practice SA solutions from LAVA and USM3D Mixed Element solvers.

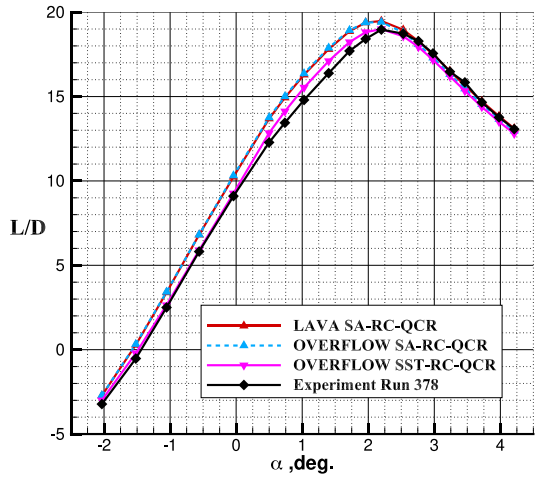

(g) L/D-α curve comparing overset grid solutions

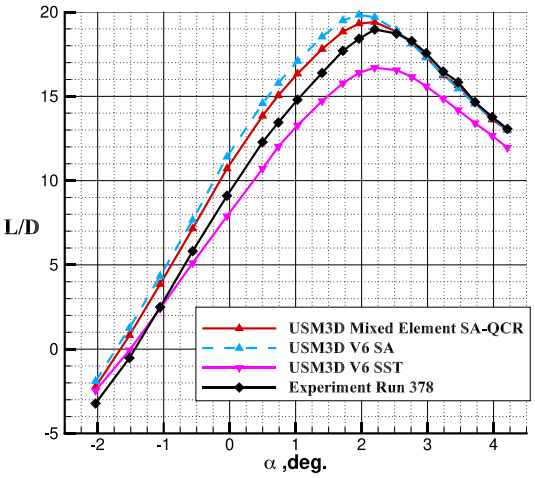

(h) L/D-α curve comparing unstructured grid solutions

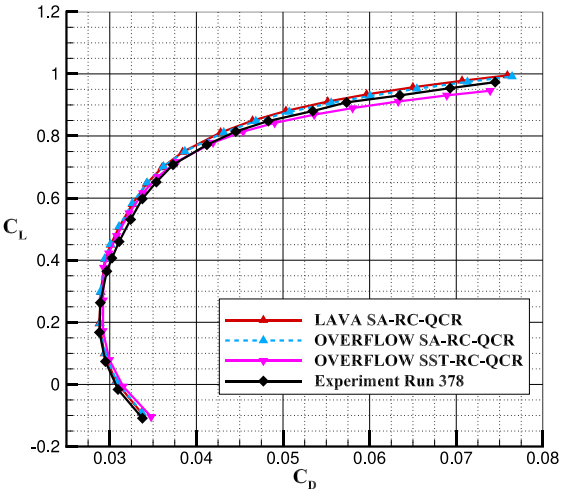

(i) Drag Polar comparing overset grid solutions

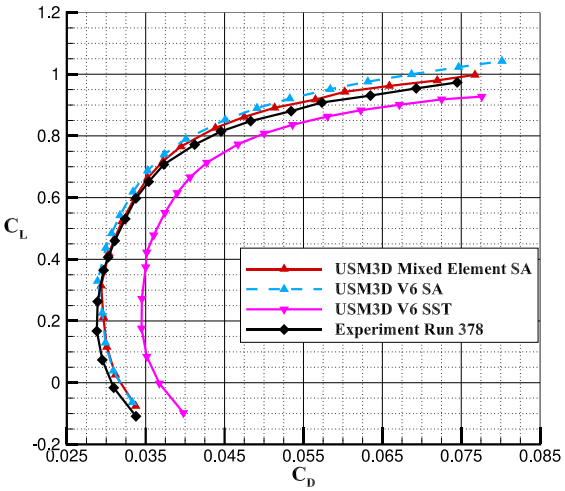

(j) Drag Polar comparing unstructured grid solutions

Fig 4 Continued. Angle of Attack Sweep at Mach 0.8 and Re = 5.25 x 10^6 / ft comparing the SA and SST turbulence models for OVERFLOW and USM3D as well as comparing those results with the best practice SA solutions from LAVA and USM3D Mixed Element solvers.

For the unstructured grids, the SA solutions behave similar to the structured solutions, a strong agreement is seen at the lower angles of attack and a larger overshoot of drag at the higher angles of attack. Above 2˚, the USM3D V6 solution predicts increased drag relative to USM3D Mixed element results. A difference peak from experimental data of 60 counts is predicted with USM3D V6, while USM3D Mixed Element sees a peak difference similar to the structured mesh results at 30 counts. At angles of attack above 3˚, USM3D V6 SST results show a similar reduction in drag as the OVERFLOW SST results. However, below that angle of attack the predicted C_D is higher than with the SA turbulence model and the shape of the C_D-α curve changes. The C_D is overpredicted at the lowest angle of attack by 60 counts, which is equivalent to a 20% increase in drag relative to the USM3D V6 SA solution. The average increase in drag up to 3˚ is 12%. In comparison, the OVERFLOW SST solution saw an average 2% increase in drag where it was predicting more drag. This peaks at an increase of 3%. This difference in drag relative to OVERFLOW solutions needs to be investigated. A look at the C_p profiles on spanwise cuts along the wing as well as flow visualization and analysis will be done in an attempt to gain a better understanding of what the cause might be.

The C_{My}-α curve when using the SST turbulence model appears to, on average, predict pitching moment closer to the experimental data. However, a lot of this decrease in error comes from the mid-range angles of attack. At low and high angles of attack the SST does not predict the pitching moment as well as the SA turbulence model. Neither the SST model nor the improvements to the accuracy of the individual solver discussed earlier in the paper seem to cause the change in the C_{My}-α curve shape that is needed to correctly predict the experimental pitching moments. This

indicates that higher-fidelity simulations might be necessary, which could include transition modeling, higher-fidelity models to properly capture shock boundary layer interaction effects, or a change in the geometric representation.

In terms of lift-to-drag ratio (L/D) versus angle of attack, for the overset grid solutions there is a significant improvement in terms of predicting the experimental curve when using the SST turbulence model. The error relative to experimental L/D is reduced when going from OVERFLOW SA to SST throughout the entire angle of attack sweep and shows showing significant improvement at the mid-range angles with an average reduction in error of 62%. For the unstructured grid solutions with USM3D V6, the larger increase in drag and low lift at high angles of attack cause the L/D curve to shift away from experimental data. There is still improvement at the lowest angles of attack.

Lastly, the OVERFLOW SST solution shows improvement over the OVERFLOW SA solution when comparing to the experimental drag polar in the range $0.4 < C_L < 0.9$. This is due to the improved C_L prediction below 3° angle of attack and improved C_D prediction above 0°. This is also the range where pitching moment was better predicted by the SST turbulence model. However, the higher drag at low angles of attack and lower lift at high angles of attack cause the remainder of the OVERFLOW SST drag polar to move away from experimental data. With the USM3D solutions, since the SST model is always overpredicting C_D, the drag polar is shifted right of the experimental data. At the point where SA and SST predict the same drag, the SST model predicts too little lift to match the experimental drag polar and the SA model results.

In an attempt to gain insight on why the SA and SST turbulence models predict different loads, and why this difference changes with grid paradigm and CFD solver, the flow solutions were investigated further.

B. Decay of Turbulent Quantities

There were no sustaining terms for the OVERFLOW or USM3D V6 simulations, therefore it is expected to see a strong decay of the turbulent quantities. A study was conducted comparing the USM3D V6 SST and OVERFLOW SST solutions at -0.041° where a line was extracted from the fuselage nose to the inlet of the domain. Both μ_t/μ and k were extracted from this line and can be seen plotted in Figure 5 as a function of x normalized by the mean aerodynamic chord of 110.286 in. The overset grids contain a much larger domain than the unstructured grids in the USM3D V6 solutions, this allows for more decay of turbulent quantities before reaching the model. At 15 chord lengths from the nose, the turbulent quantities begin to rise. These quantities were extracted at this location and are show in Table 6. From these values it can be see that the decay causes 1.2x decrease in μ_t/μ and 11x decrease in k for the OVERFLOW solutions. The effects of this decay will be investigated in future simulations. However, it is important to note that the differences between the freestream and near-body turbulent quantities in the OVERFLOW solutions are less than the range of quantities investigated in the turbulence intensity sensitivity study presented in Section VI A.

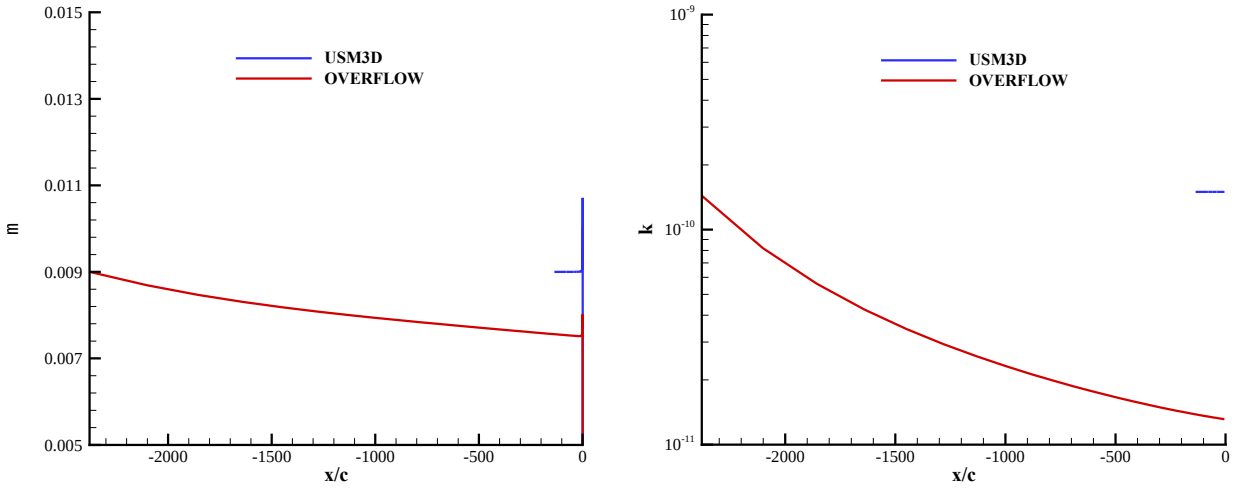

(a) Visualization of μ_t/μ decay over domain (b) Visualization of k decay over domain

Fig. 5 Decay of turbulent quantities for SST simulations at α = -0.041°, Mach 0.8, and Re = 5.25 x 10^6 / ft.

Table 6. Decayed Turbulent quantity measured 15 chord lengths away from model nose.

	OVERFLOW SST	USM3D V6 SST	OVERFLOW SST Percent Reduction
Turbulent Viscosity Ratio	0.00751	0.009	16.6%
Turbulent Kinetic Energy	1.371e-11	1.498e-10	90.8%

C. Turbulent Flow Field Comparison

An effort was made to understand the differences in turbulent flow fields of the SA and SST solutions for both the OVERFLOW and USM3D V6 solvers. This analysis compared both turbulent kinetic energy and turbulent viscosity ratio at α = -0.041° and 4.21°. The SST solutions had a higher turbulent viscosity ratio than the SA solutions and went further downstream of the wing. The highest turbulent viscosity ratio was found in between the flap hinge fairings located at and just inboard of the strut junction. A large difference in the solutions was caused by the unstructured grids diffusing the turbulent viscosity to the surrounding area. Possibly due to this same difference in the grid, the turbulent kinetic energy for the SST solutions propagates further downstream with the OVERFLOW cases. Figure 6 demonstrates this effect on turbulent kinetic energy on a x-plane slice behind the wing.

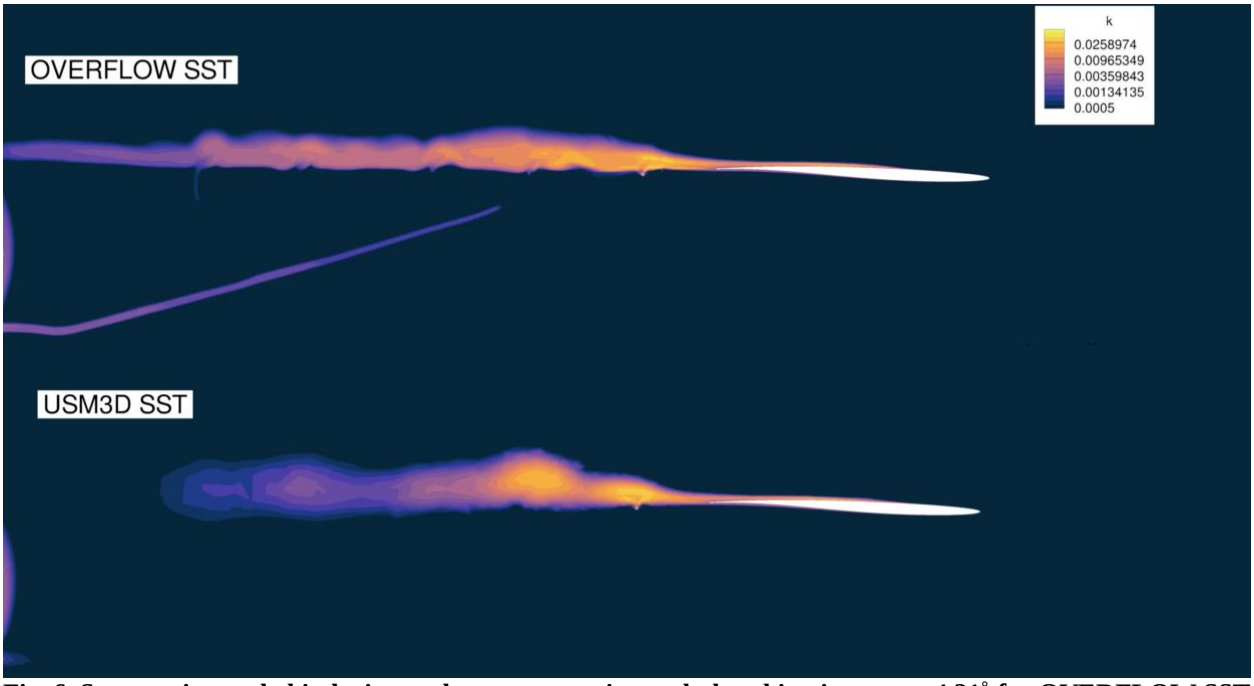

Fig. 6 Streamwise cut behind wing and strut comparing turbulent kinetic at α = -4.21° for OVERFLOW SST and USM3D V6 SST solvers.

D. Surface Contours of Pressure Coefficient

Surface contours of C_p were investigated to determine where the flow is separating or recirculating. To achieve this, surface streamlines based on the velocity vectors are added to the contour plots. 500 streamlines are initialized consistently between all the cases. An additional 50-100 streamlines are added on a case-by-case basis to help show structures or capture regions with increased separation. The SA and SST turbulence models are compared at angles of attack of -2.033°, -0.041°, and 4.21° for the USM3D V6 and OVERFLOW solvers. LAVA results using SA-RC-QCR are also included to determine where the OVERFLOW solution is predicting the same surface contours as well as what the cause of differences in drag and lift might be at low and high angles of attack. Figure 7 compares the upper surface of the wing for the angle of attack of -2.033°. Starting with a comparison of the turbulence models, the SST predicts lower pressure on the upper surface of the wing along the spanwise location of the pylon. Moving past the 3rd flap hinge fairing the SA model starts to predict a more negative pressure. The USM3D V6 and OVERFLOW SST results show very similar pressure profiles on the upper surface of the wing with the USM3D showing slightly higher negative pressure near the wing tip. The USM3D V6 SA solution predicts a consistent increase in negative pressure along the upper surface of the wing relative to the OVERFLOW SA solution. Both USM3D results predict more negative pressure on the upper surface of the strut near the strut junction. LAVA and OVERFLOW SA show no differences. Moving on to the next angle of attack of -0.041° in Figure 8, a similar relationship between the models and solvers emerges. The SST predicts less suction on the upper surface of the wing but now throughout the entire region. There are no noticeable differences between OVERFLOW and USM3D V6 SST besides a slight increase in pressure in the OVERFLOW solution near the fairing. The spanwise location of the largest region of negative pressure is near the first flap hinge fairing inboard of the strut junction. This shifts slightly inboard for the SA turbulence model

results. The USM3D V6 SA model continues to predict lower pressure over the upper surface of the wing. LAVA SA results again match OVERFLOW. Figure 9 shows the upper surface of the wing at a 4.21 angle of attack. On all plots it is clear where the shock is forming on the upper surface. Behind it the region of reverse flow shows separation is occurring. With the SST turbulence model this shock is occurring much earlier than with the SA solution. This would cause the decrease in lift seen in the angle of attack sweep curves for both solvers. All of the simulations are experiencing the earliest shock slightly inboard of the strut junction. For the SA solutions the flow after the shock remains relatively clean with very little movement in the spanwise direction. For the SST solutions there is more crossflow from root to tip. This is very apparent in the USM3D V6 SST solution near the wing fairing where the flow after the shock appears to be moving sideways from root towards tip. Additionally, at the region behind the early shock there is recirculation occurring on the upper surface of the wing. With these features and the earlier prediction of shock, the USM3D V6 SST solution no longer matches as well with the OVERFLOW SST solution for the upper surface of the wing. Outboard of the strut junction the SST solution flow patterns are similar, predicting a slightly larger region of circulating flow near the tip than the SA solutions. However, even in this region the solutions differ as seen with the streamlines. The USM3D V6 SA solution predicts the aft-most shock and also has the least crossflow but otherwise compares well with OVERFLOW SA. LAVA SA matches OVERFLOW SA for most of the upper wing surface with the exception of predicting slightly higher pressure near the trailing edge just outboard of the pylon.

Moving on to the underside of the wing, Figure 10 compares the solutions at -2.033°. All results show a recirculation region inboard of the pylon. At the start of the recirculation is a section with higher pressure than the surrounding leading-edge portions of the bottom surface. It was noticed in unconverged spurious solutions that this region would peak in negative pressure before increasing in pressure and developing into recirculation. There are two additional recirculation zones. The first one occurs outboard of the second to last flap hinge fairing but is only present in the SST solutions. The SA solutions have some reverse flow near this region but do not show recirculation. The second exists in the USM3D V6 SST solution inboard of the strut flap hinge fairing. The USM3D V6 SA solution has a tiny recirculation region there. Neither OVERFLOW solutions show this recirculation. With regards to surface pressure the SA solutions show higher pressure near the trailing edge. In particular just inboard of the strut junction. Figure 11 shows the lower surface of the wing at -0.041°. The recirculation inboard of the pylon still exists in most of the simulations and has shrunken in size. In the region near the recirculation the correlation with pressure at the junction surface and size of recirculation can be seen. USM3D V6 SST has the largest circulation region and it has pushed the low-pressure region further towards the root. The OVERFLOW SST solution has done this to a lesser extent. For the OVERFLOW SA and LAVA solutions this region inboard of the pylon still has lower pressure with a corresponding smaller recirculation region. For the USM3D solution there is a much lower pressure peak near the pylon junction and therefore much less noticeable recirculation and separation of the flow. The outboard side of the pylon experiences an inverse effect where the higher the pressure is on the inboard section the lower it is on the outboard. Continuing to look at the lower surface contours, the trailing edges for both the wing and strut of the SA solutions experience higher pressure than the SST solutions. In particular the USM3D V6 SA experiences the highest pressure while the USM3D V6 SST experiences the lowest pressure. Figure 12 shows the lower surface of the wing and strut for the angle of attack of 4.21°. Inboard of the second flap hinge fairing the SST solutions match well with each other as do the SA solutions. The SA turbulence model is again predicting higher pressure on the strut trailing edge. Between outboard of the second flap hinge fairing there are many more differences among the solutions. Figure 13 closes in on the problematic region. The OVERFLOW solutions have peaks and valleys originating from the trailing edge of the wing. This is more noticeable with the SST solution. The LAVA does not experience this behavior like OVERFLOW SA. Looking back at the USM3D solutions, these are predicting lower pressure near the mid region of the wing. The USM3D V6 SST has the lowest pressure in this region and also appears to have circulation zone outboard of the third flap hinge fairings. None of the other solutions predict similar features.

To summarize, the SST solutions seem more sensitive to the shock as well as the pylon/flap hinge fairings interaction with the wing. They are more likely to have recirculation on the underside of the wing. They predict lower lift due to the decreased suction on the upper surface of the wing and do a better job predicting the pressures on the lower surface trailing edge. USM3D seems to predict the highest pressures on the underside of the wing and strut and lowest pressure on upper surface which corresponds to its higher lift values. OVERFLOW SA and SST show smaller differences, earlier shock in the SST solutions account for some of the reduction in lift seen in results. LAVA results match well with OVERFLOW SA but at high angles of attack OVERFLOW SA predicts disturbances in the flow near strut junction not observed in the LAVA simulations.

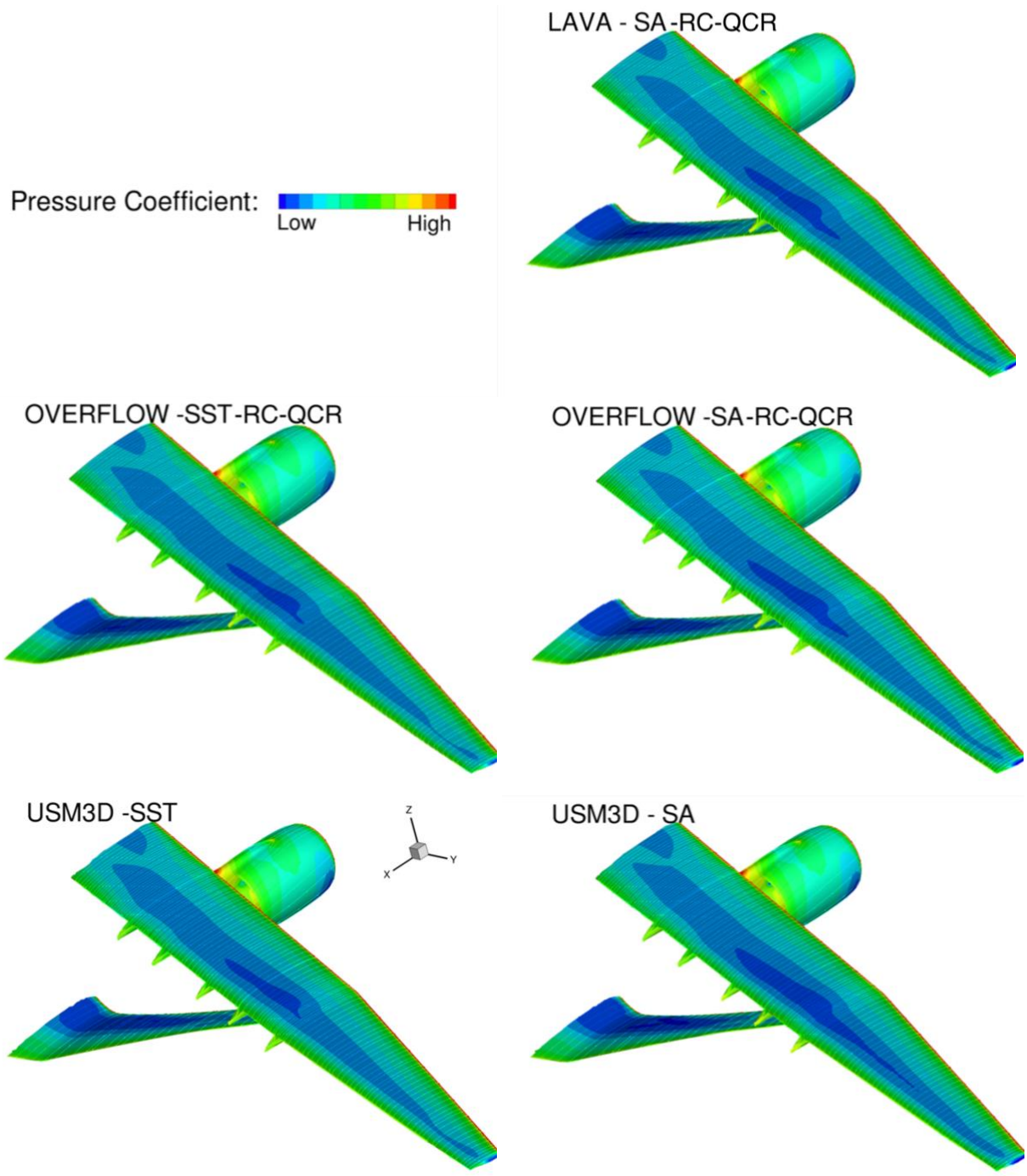

Figure 7. Upper Surface of WBSNFV Configuration at α = -2.033°.

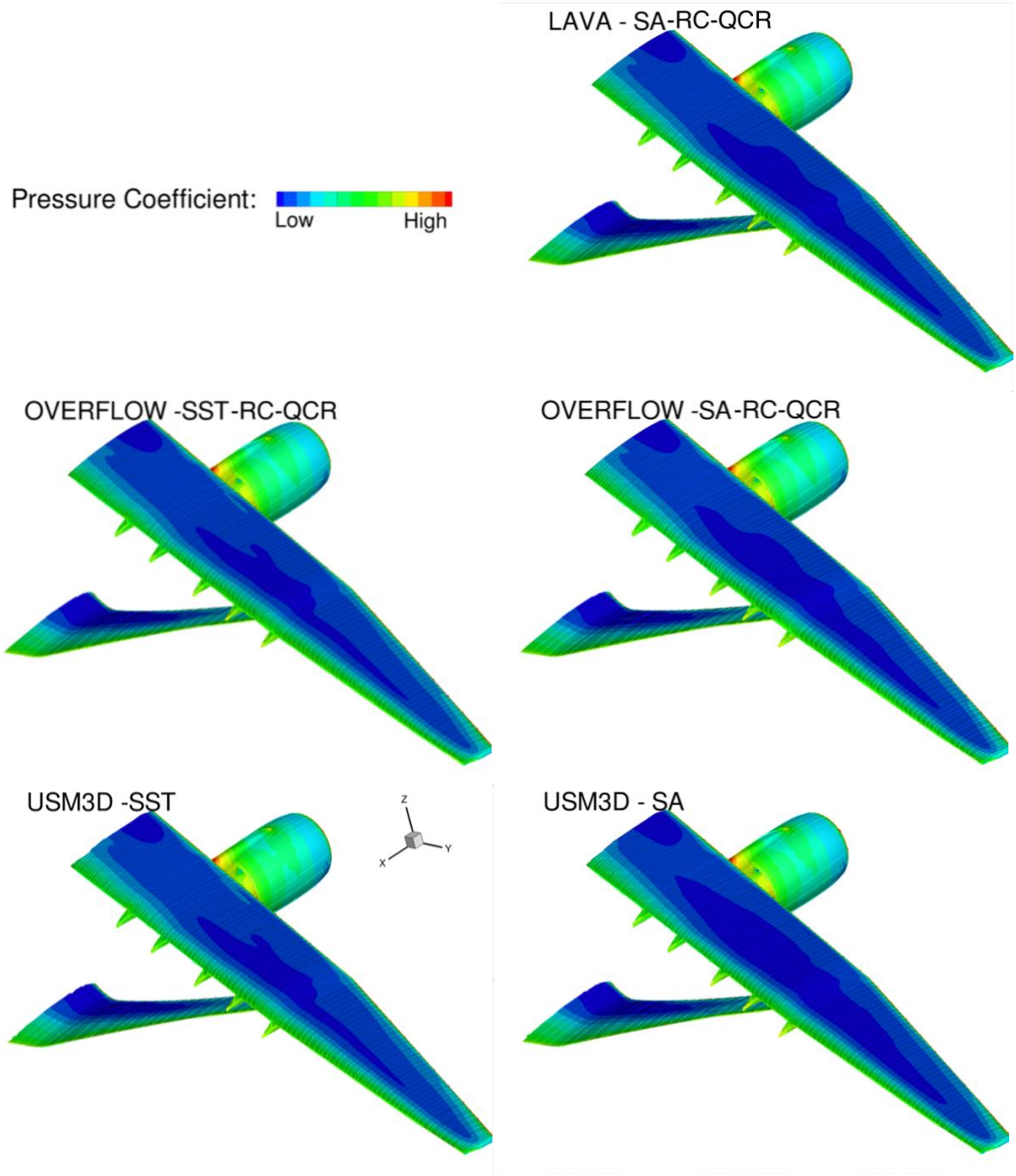

Figure 8. Upper Surface of WBSNFV Configuration at α = -0.041°.

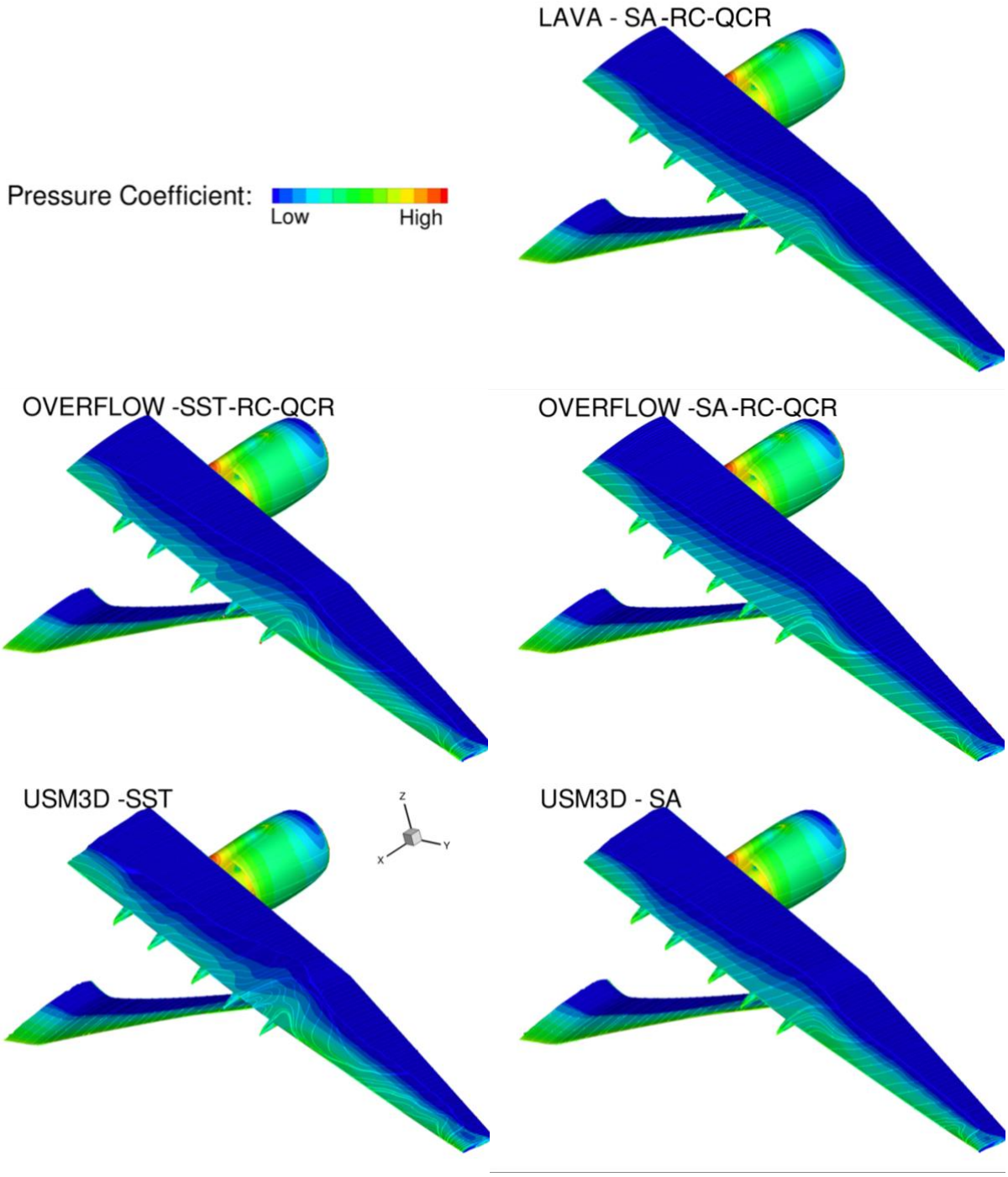

Figure 9. Upper Surface of WBSNFV Configuration at $\alpha = 4.21^{o}$.

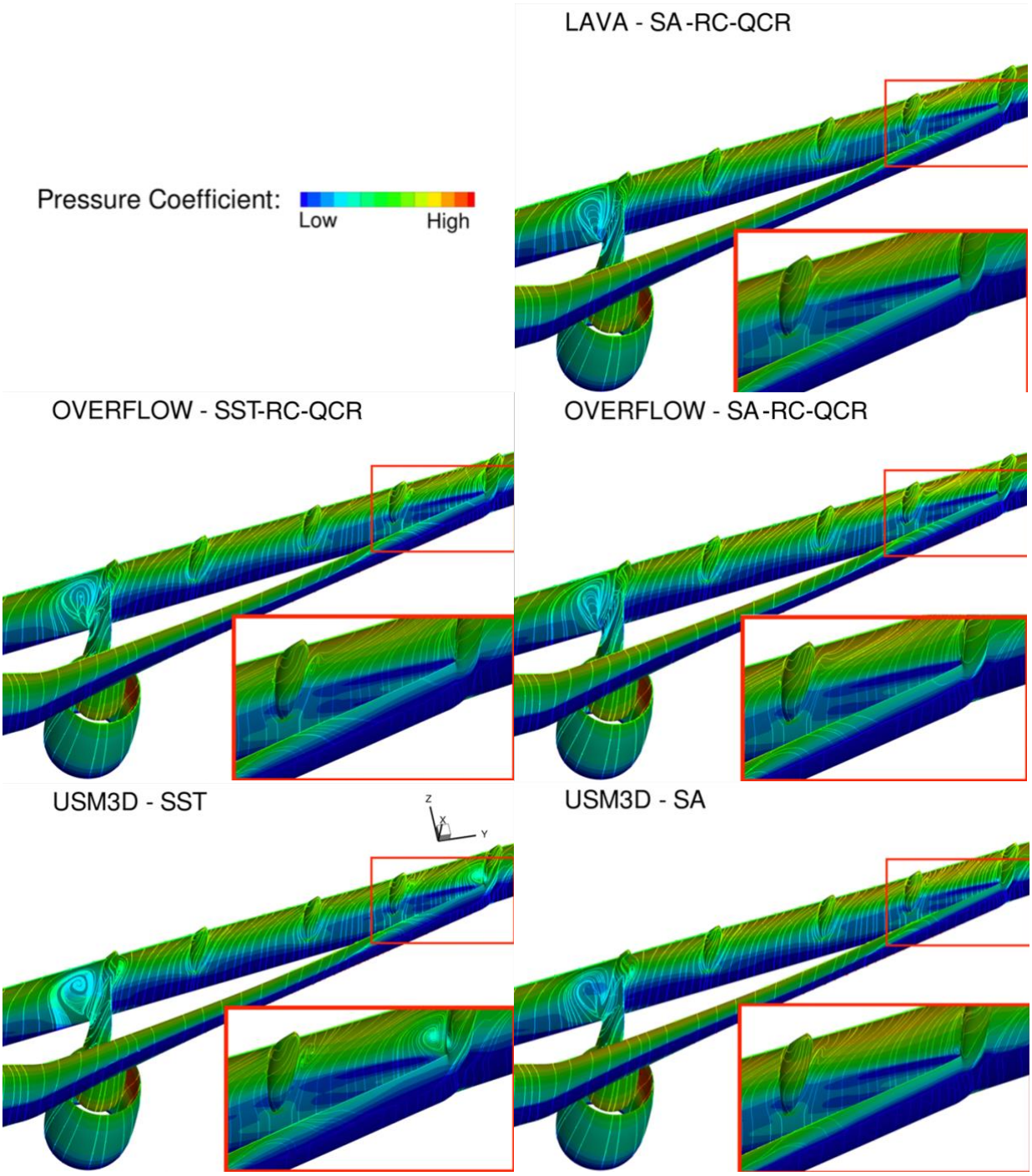

Figure 10. Bottom Surface of WBSNFV Configuration at α = -2.033°.

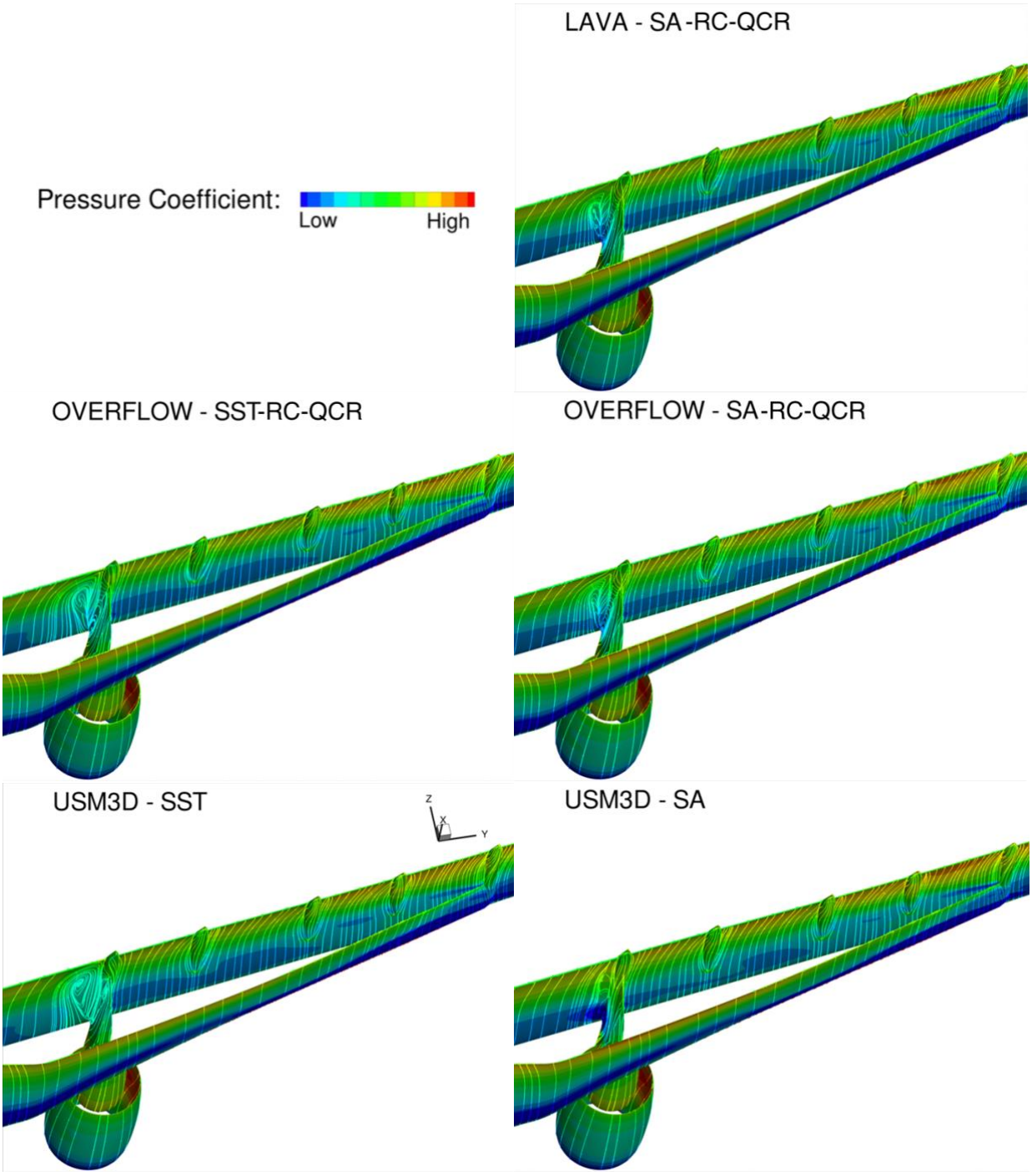

Figure 11. Bottom Surface of WBSNFV Configuration at α = -0.041°.

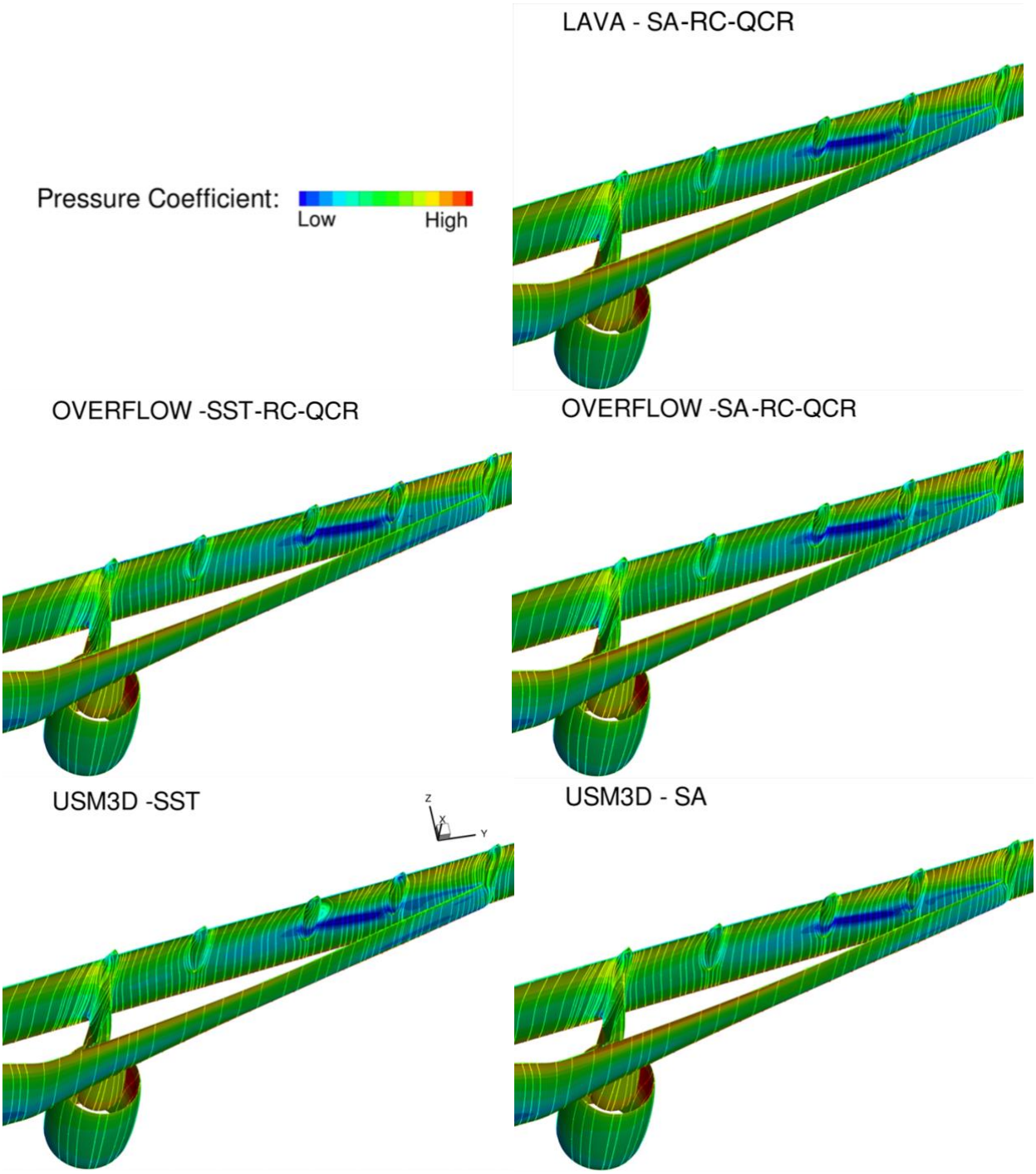

Figure 12. Bottom Surface of WBSNFV Configuration at α = 4.210 °.

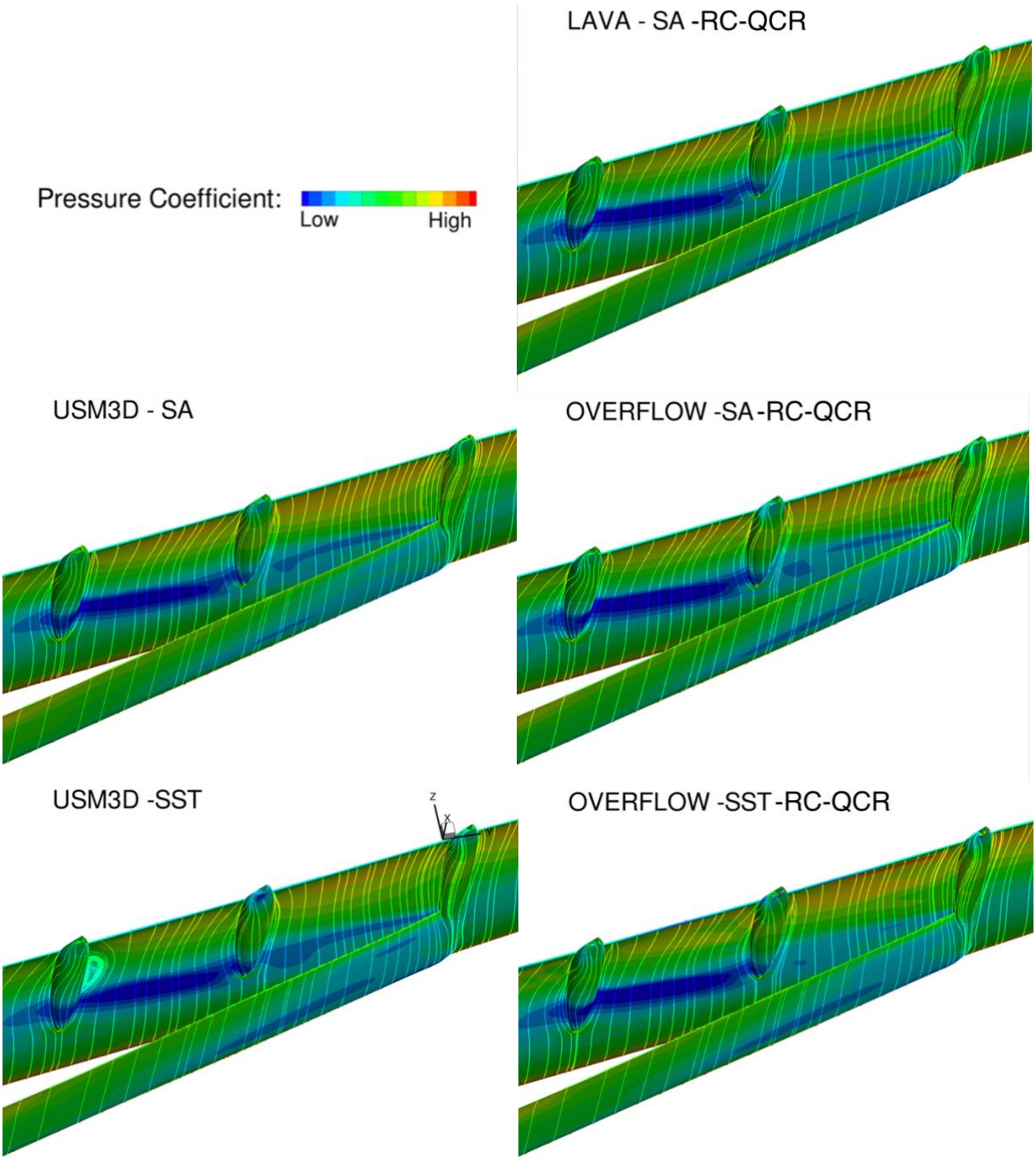

Figure 13. Bottom Surface Near Junction of WBSNFV Configuration at $\alpha = 4.210^{o}$.

E. Skin Friction Analysis

There is a 20% increase in drag for the USM3D V6 SST results. The C_p surface contours do not show what could account for that increase. A look into previous papers showed a case where the USM3D V6 SST turbulence model predicts a large increase in skin friction relative to the SA solution as well as increase in drag [25]. Figures 14 and 15 compare the skin friction between the SA and SST turbulence model for USM3D V6 Solver. There is a clear increase in skin friction near the leading edges as well as on the fuselage body. Since the SST model was overpredicting drag at lower angles of attack but predicting less drag at the highest angle of attack the skin friction alone does not explain that behavior. The drag at several angles was decomposed into pressure and viscous drag. These values can be seen in Table 7. At low angles the larger separation around junctions is likely to be having a large contribution to the increase in pressure drag. The general increase in skin friction from the SST turbulence model explains why for a range of angles of attack there is a consistent 38-40 viscous drag count contribution, and the decrease in pressure drag at the higher angle of attack makes it possible for SST simulation to have similar or lower drag than SA.

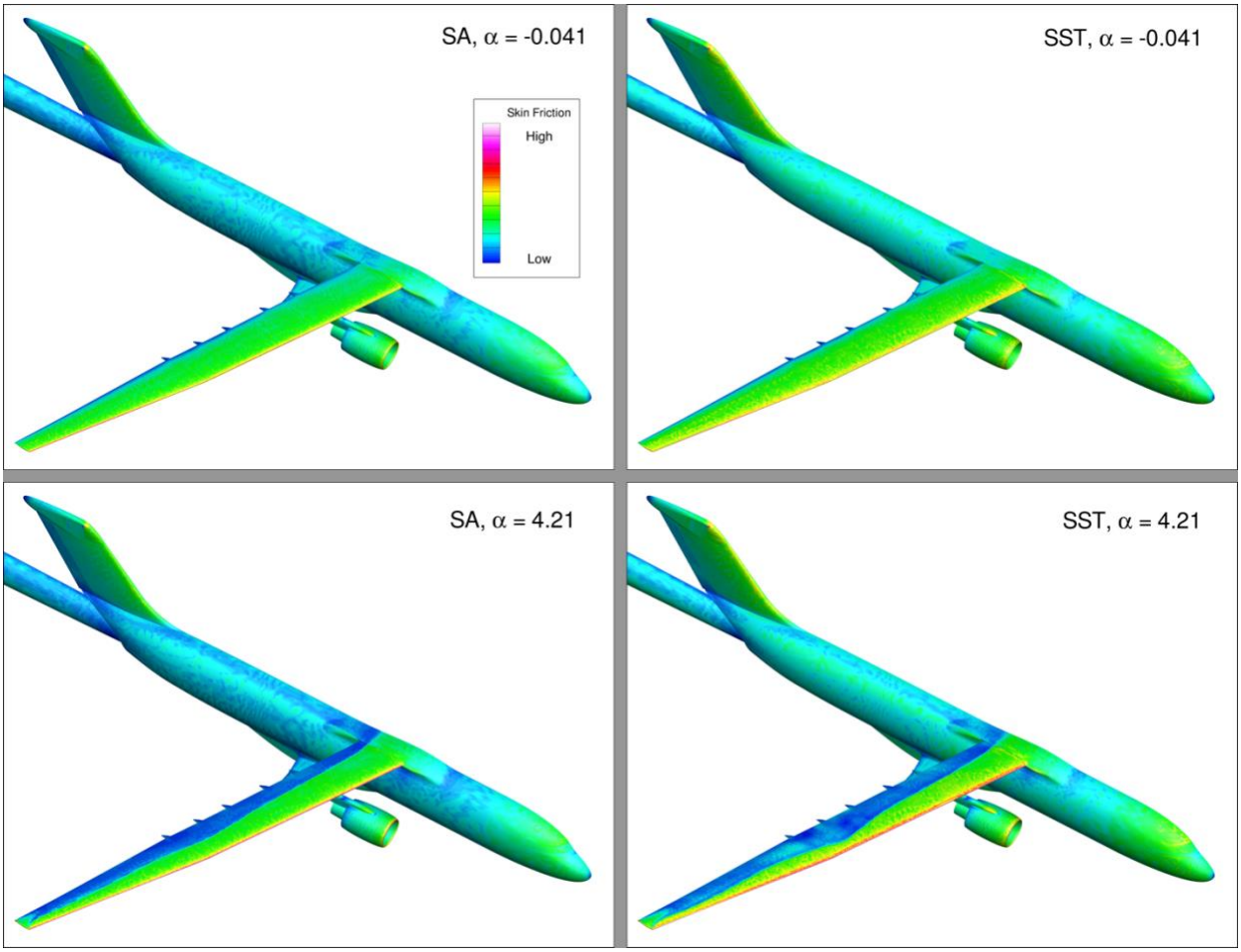

Figure 14. USM3D V6 computed skin friction on TTBW model at α = -0.041° and 4.21°.

Table 7. Breakdown of drag increase from SST turbulence model for USM3D V6 solution.

Angle of Attack	Viscous Drag Counts	Pressure Drag Counts	Total Drag Counts
-2.033	38	26	64
-0.041	40	16	56
2.9796	40	-36	3.5

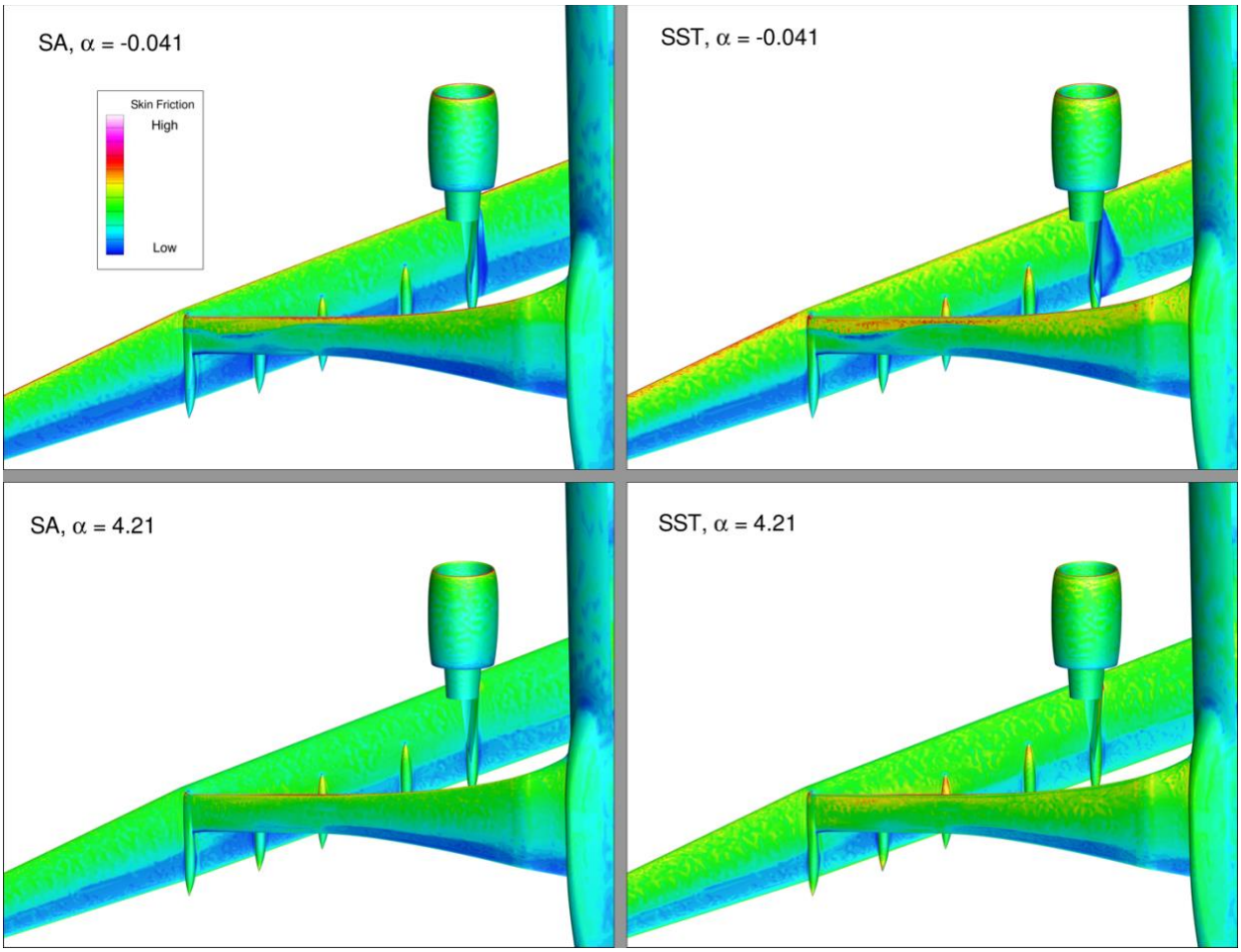

Figure 15. USM3D V6 computed skin friction on bottom surface of TTBW at α = -0.041° and 4.21°.

F. C_p Profiles

To get a more quantitative understanding the differences in loads, C_p profile spanwise cuts of the wing and strut are extracted from the flow solution and compared. The initial comparison is between the SA and SST solution of the USM3D V6 and OVERFLOW solvers at angles of -2.033°, -0.041°, and 4.21°. These results are plotted against experimental data from run 378. While the best practice for TTBW C_p plots is to target the C_L from experimental data, comparing SA and SST based on the angle of attack will be more useful in showing the improvement gained if any by using one of the turbulence models. This initial comparison of the C_p profiles can be found in Figure 16-18.

Starting with the angle of attack of -2.033° and looking at the wing profiles, the largest differences are seen on the lower surface at eta stations 7.2% and 24%, which correspond to inboard and outboard of the pylon junction where the separation was seen to occur. On the upper surface, the solutions match relatively well with the SST model predicting more negative pressure further downstream than SA, but both the SA and SST overpredict experimental negative pressure in this region. There is less variation between the codes at stations 37.3% and 49.6.%. In these regions the SST model is predicting less negative pressure on the upper surface providing a slight improvement in matching experimental results. The SST solutions, in particular the USM3D V6 SST solution, do a better job at matching experimental C_p near the trailing edge of the bottom surface. In these regions the SST solutions are predicting a recirculation region where the SA solutions do not. In between the strut junction the flap hinge faring there appears to be channel-like flow with a shock-expansion wave train, which is causing oscillations in the C_p profile. As seen earlier in the flow solution, the USM3D V6 SST solution experiences a recirculation region near the strut-wing junction, which causes a large mismatch with experimental data. While USM3D V6 SA solution did predict a small

amount of separation, it does not show a strong deviation from the experiment. Further outboard on the wing, there are no longer significant differences between the SA and SST solutions on the underside of the wing with the exception of the higher-pressure prediction by the SA model near the trailing edge. On the upper surface, the SST model predicts slightly lower pressure. Looking at the strut for this angle of attack at station 7.2% the USM3D V6 SST predicted performance does not do as good a job in matching experimental data. At station 11% there is essentially no difference between the cases. At station 24% the SST solutions continue to predict lower pressure on the lower surface trailing edge and in that region, there is the largest amount of spread between the solutions.

Looking at angle of attack of -0.041° at the most inboard station, all the cases lie on top of each other with the exception of the USM3D V6 SST solution near the quarter chord of the bottom surface. This increase in pressure could be related to the stronger recirculation occurring inboard of the pylon. At station 24%, just as in the previous angle of attack, there is a high variance between all of the solutions on the lower surface of the wing, and in both cases the OVERFLOW SA solution has done the best job at matching experimental C_p in that region. On the upper surface of the wing the USM3D V6 SA solution is generating significantly more suction which was noted in the flow solution earlier. This overprediction of negative pressure on the upper surface of the wing continues past the most outboard station. For all the stations outboard of station 24% the SST models do a better job at matching experimental data. The USM3D V6 SST continues to perform best at the lower surface trailing edge.

At the highest angle of attack near the root, the solutions are similar except for the shock location. Both SST models do a good job predicting the shock location, while the SA models both predict the shock aft of experiment. The continuous drop in the solution hints that the solution is fully separated after the shock. At 37% the SST models continue to accurately predict the shock location. The OVERFLOW SST solution experiences oscillations in C_p near the trailing edge of the lower surface, this oscillation exists up to the strut junction where the OVERFLOW SA solution is also seeing these effects. At station 49.6%, the USM3D V6 and OVERFLOW SST solutions no longer agree with the predicted shock location. OVERFLOW SST predicts similar shock locations with respect to the OVERFLOW SA solution, while the difference between USM3D SST and SA shock location increases. At 55.4% the predicted shocks are closer together and OVERFLOW SST still predicts the location well. At the last two stations, the USM3D V6 SA solver predicts the shock well and the two SST solvers converge to similar profiles. For the strut, there is no large difference between the solutions, which all do a good job at predicting the shock over the upper surface of the strut.

G. C_L Targeting

Studies performed on the TTBW have shown that when the simulations are run at the corresponding C_L value, the C_p matches closer with experimental data than if run at the corresponding alpha. This is due the alpha shift seen in the C_L-α curves. A look at this shift can also tell how close the solutions are to experimental data. Table 8 shows some of the loads and angles of attack for the SA and SST solutions using OVERFLOW and USM3D V6. Based on these results, for given lift the drag from the OVERFLOW solutions lie within the USM3D V6 SA and SST values. There is an 8 drag count difference for OVERFLOW and 68.4 drag count difference for USM3D between the two turbulence model solutions. Due to this large increase in drag the C_D values do not match between SST solutions, but the pitching moment and angle of attack are very similar, with a 1.75% difference in pitching moment and 0.75% difference in angle of attack. The C_p profiles for this data along with the LAVA SA and USM3D Mixed Element SA results are plotted in Figure 19. Comparing LAVA with the OVERFLOW SA solutions it appears that the LAVA profile deviates at and after the shock location. In general LAVA does a better job at predicting the shock location than the same grid simulated with OVERFLOW. In terms of USM3D Mixed Element and USM3D V6, the mixed element solver consistently does a better job on the upper surface of the wing predicting higher suction at the plateau, an earlier shock location, and less pressure post shock.

Table 8. Corresponding loads and angles for cases targeting C_L = 0.7074.

Variable	Experimental	OVERFLOW SA	OVERFLOW SST	USM3D V6 SA	USM3D V6 SST
C_D	0.0373	0.0364	0.0372	0.0356	0.0424
C_{My}	-0.1337	-0.1635	-0.1423	-0.1883	-0.1448
α	2.198	1.9852	2.1501	1.8073	2.1665

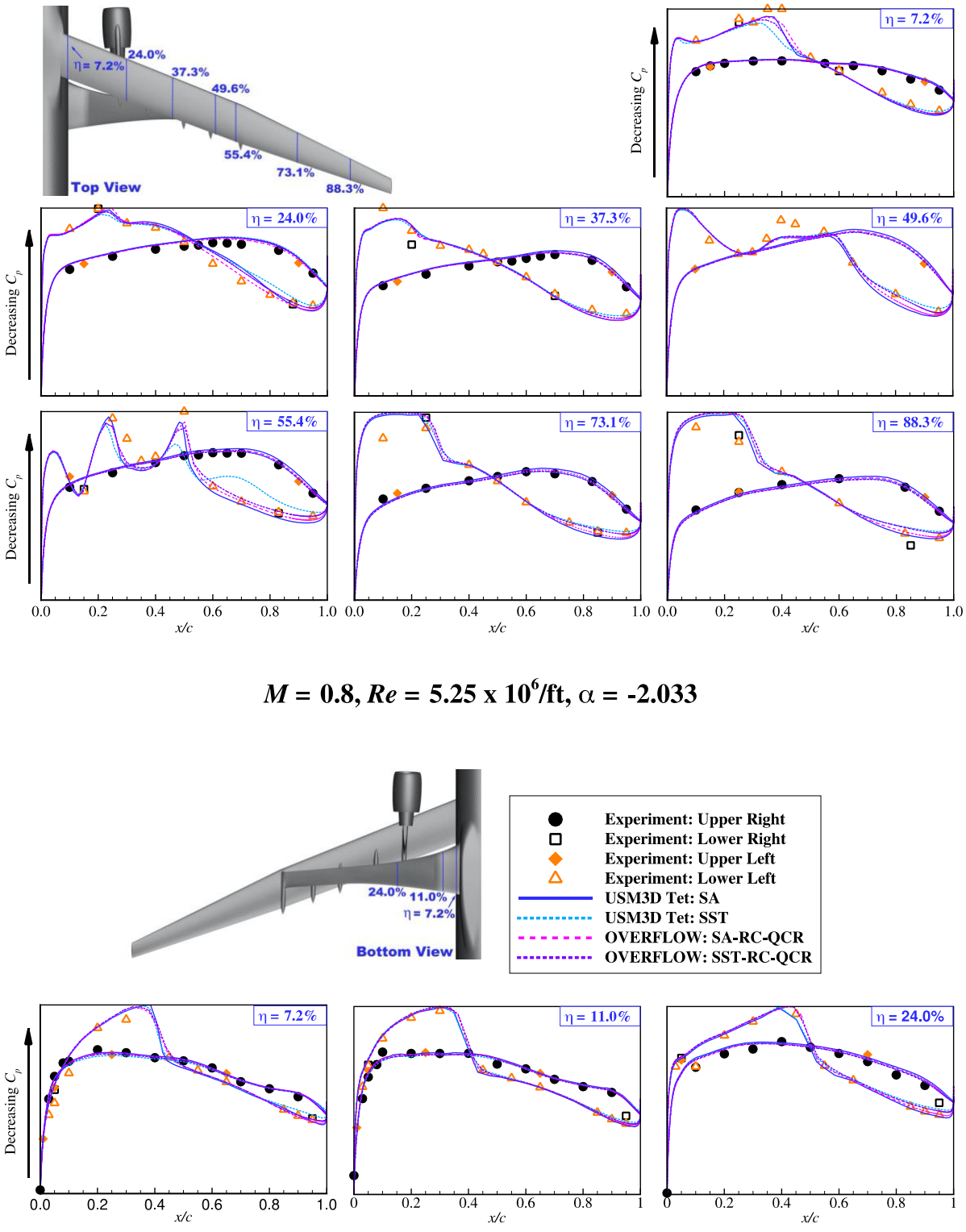

Figure 16. C_p profile spanwise cuts on wing and strut for WT WBSNFV Configuration at α = -2.033°.

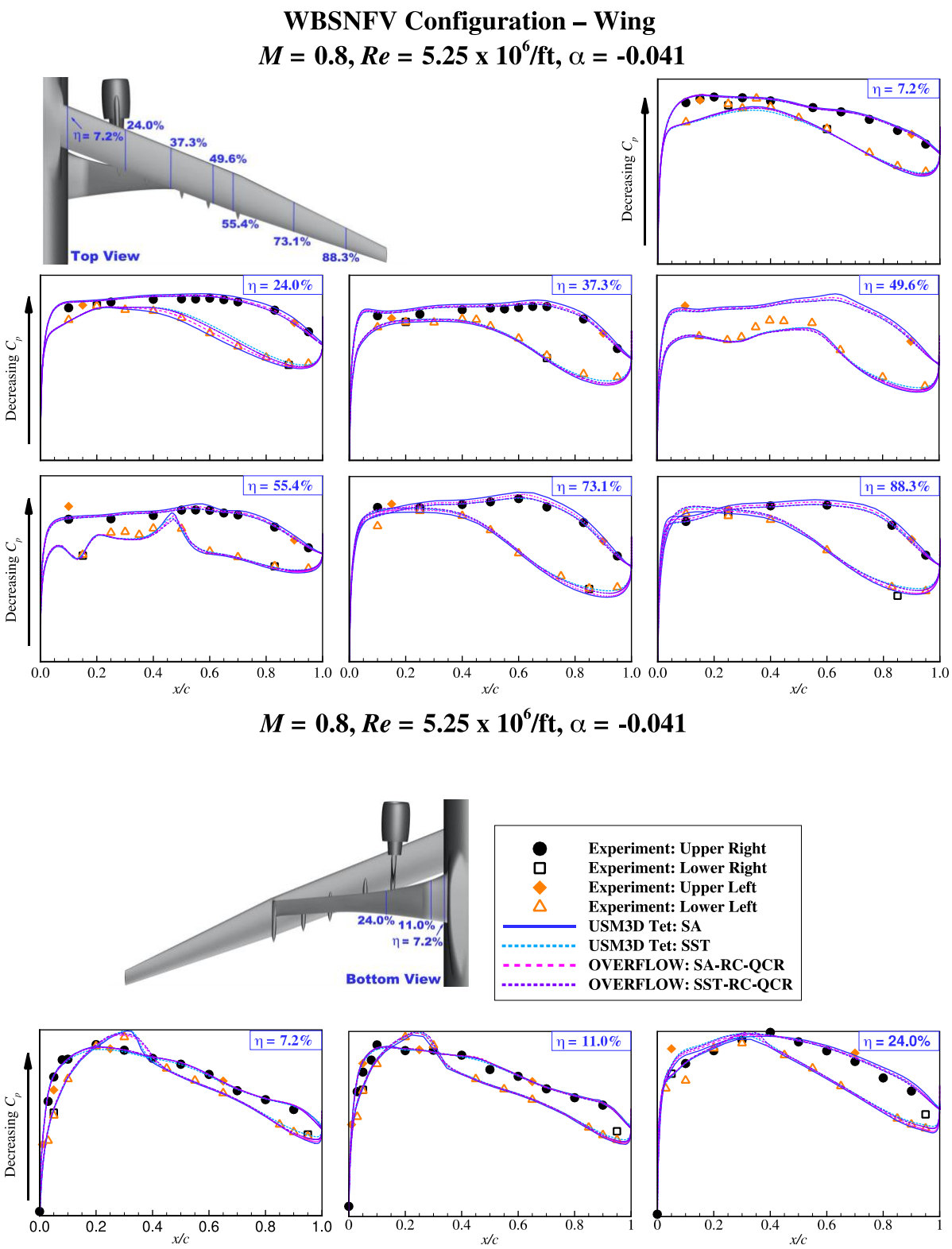

Figure 17. C_p profile spanwise cuts on wing and strut for WT WBSNFV Configuration at $\alpha = 4.21^{o}$.

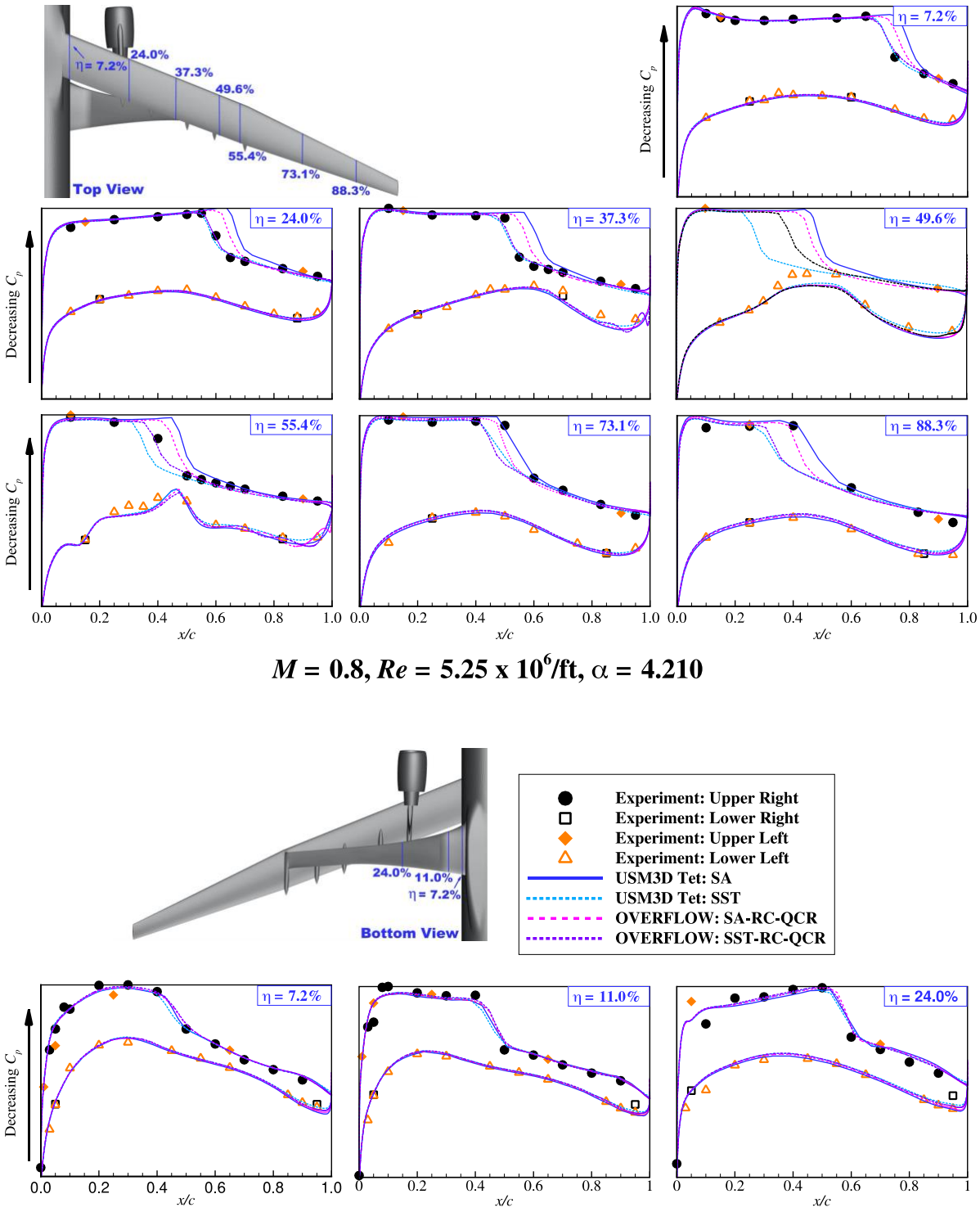

Figure 18. C_p profile spanwise cuts on wing and strut for WT WBSNFV Configuration at α = 4.21°.

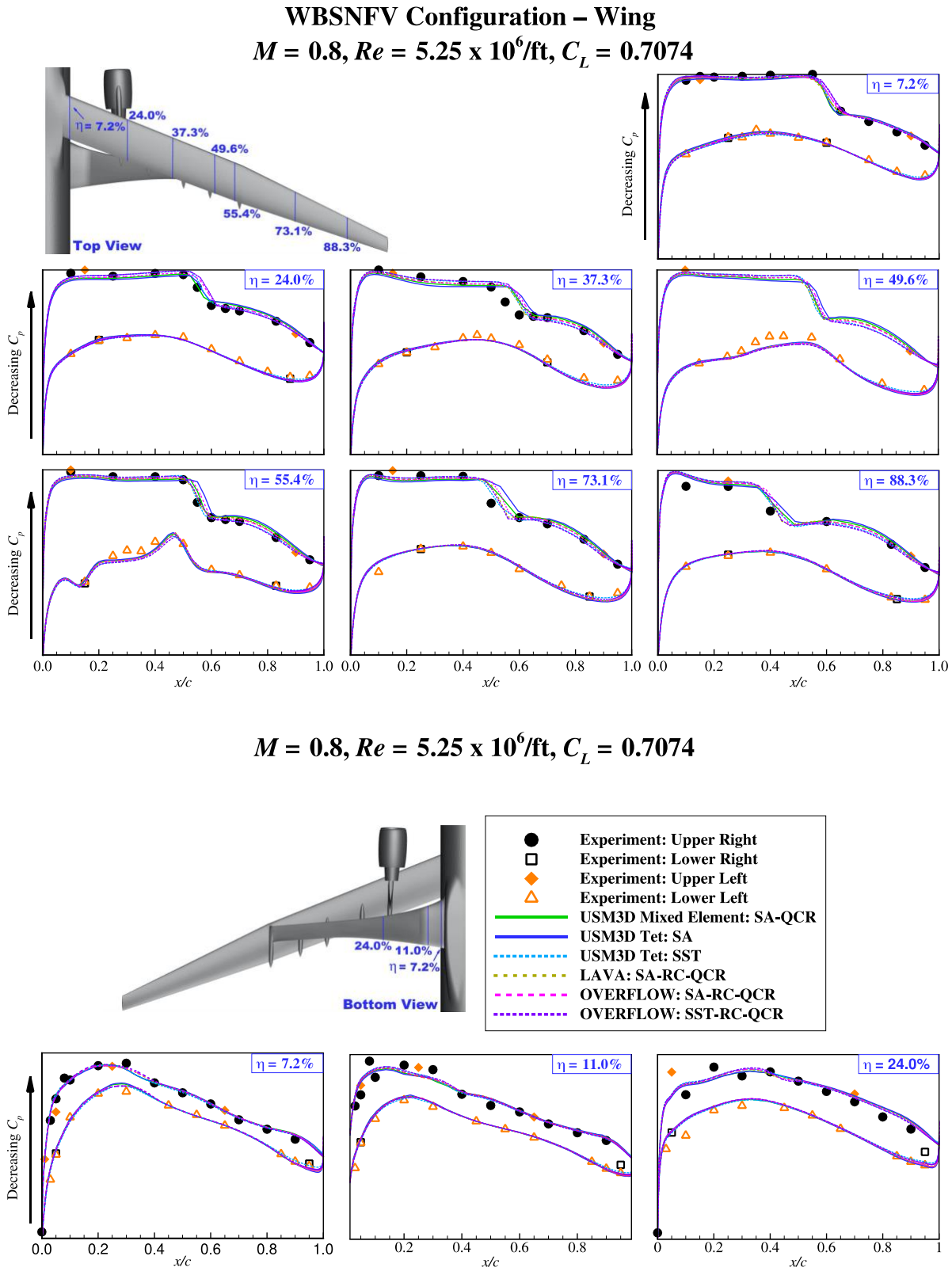

Figure 19. C_p profile spanwise cuts on wing and strut for WT WBSNFV Configuration at C_L = 0.7074.

H. Structured Overset Resource Utilization

To conclude this section, a comparison of resources required to perform the structured overset simulations is presented. Table 10 compares the resources used for the -0.041 angle of attack for LAVA and OVERFLOW using the SA turbulence model on the same structured overset mesh. Compared to OVERFLOW 2.2n with overrunmpi there is an 8x reduction in resource cost with the refactored LAVA solver, with the LAVA solver demonstrating significantly improved residual convergence. This is one of the motivations to continue implementing SST in LAVA, and a SA vs SST comparison using LAVA will be presented in future work.

Table 10. Resource comparison between LAVA and OVERFLOW.

Solver	Turbulence Model	CPUs	Nodes	Architecture	Walltime (hours)	Conversion Factor	Total SBUs
LAVA	SA	2000	50	Skylake	0.55	1.59	43.725
OVERFLOW	SA	840	30	Broadwell	12.3	1.00	369.00
Improvement							8.44

VIII. Conclusion

The goal of this paper was to narrow the gap between CFD predictions of aerodynamic performance of the Mach 0.80 TTBW and experimental results. This effort was attempted by two different means: the improvement of the solvers with the aim of producing a more accurate solution, and the utilization of the k-ω SST turbulence model.

Comparison between production LAVA and refactored LAVA shows improvement in accuracy for all loads by reducing load standard deviation by 2-10x, as well as improving residual reduction by 2-35x. In terms of comparison with the experiment, when using refactored LAVA instead of production LAVA the average difference from experiment was reduced from 15% to 8% for C_L, C_D from 27 to 8 drag counts, and from 25% to 12% for C_{My}. Additionally, refactored LAVA shows reduction in resource cost of 1.5-4x for these TTBW free air simulations. For USM3D, the difference in experimental loads, when using USM3D Mixed Element as opposed to USM3D V6, is reduced from 18% to 13% for C_L, C_D from 25 to 16 drag counts, and from 25% to 15% for C_{My}. USM3D Mixed Element also shows a 7-10x speedup when compared to USM3D V6. Overall, the improvement of the codes increased the accuracy of CFD predictions and reduced the required resources.

Since SST was not implemented in LAVA, OVERFLOW was used to run SST as well as SA for a better understanding of the sensitivity to turbulence model. LAVA and OVERFLOW SA predict the same loads for the investigated angle of attack sweep with max error of 0.5%. This difference between the solvers occurred at the higher angles of attack where the OVERFLOW solutions did not experience the same level of convergence as LAVA. In terms of speed, LAVA shows about an 8x speedup when compared to running OVERFLOW with the same number of cores using MPI.

The effect of using the SST turbulence model varies between the solvers. Both USM3D V6 SST and OVERFLOW SST solutions show improvement in predicting C_L. At high angles of attack the SST solutions underpredict C_L but the difference with experimental data is still reduced. In terms of C_D, the SST model overpredicts drag at the lower angles of attack and shows improvement over SA at the highest angles of attack. For OVERFLOW, the SST predicts an additional 10 drag counts or 3% relative to the SA solution at the lowest angle of attack. This error is reduced as angle of attack increases and at 1.5 degrees the SST model start predicting drag closer to experiment than the SA model. For USM3D V6, the SST predicts an additional 60 drag counts or 20% relative to the SA solutions. This increase in drag is caused by an increase in viscous drag of approximately 40 counts throughout the entire angle of attack sweep. This appears to be caused by an increase in skin friction from using the SST model. At 3 degrees angle of attack the SST model predicts less drag than the SA model due to a significant drop in pressure drag relative to the SA solution. For pitching moment, the SST model matches better with experimental data in the mid-range of angles of attack. In terms of the drag polar, both OVERFLOW SST and USM3D SST fail to match experimental data at low and high C_L values. This is due to the drag increase at low angles of attack and the underprediction of lift at high angles of attack. In terms of computational cost, the OVERFLOW SST solution is 1.44X more expensive, on the test case run, than the OVERFLOW SA. In conclusion, the SST model does show an improvement for predicting C_L for both OVERFLOW and USM3D, but the results do not demonstrate improvement across all loads consistently, and thus remain inconclusive pending further studies. Higher-fidelity simulations might be necessary, which could include transition modeling, higher-fidelity models to properly capture shock boundary-layer interaction, or a change in the geometric representation.

Acknowledgments

This research has been funded by the NASA Advanced Air Transport Technology Project under the High Aspect Ratio Wing Subproject. Refactoring of LAVA solver has been partially funded by the Transformational Tools and Technologies (TTT) , Commercial Supersonic Technology (CST), and AATT Projects. Computer resources were provided by the NASA Advanced Supercomputing (NAS) facility. The authors would like to thank and acknowledge Jared Duensing and Ercan Dumlupinar for their guidance and assistance with the simulations, Gerrit Stich for his contributions to the implementation of k-ω turbulence to the LAVA framework, and lastly the entire Boeing team through the research conducted under the NASA BAART contract NNL16AA04B and Greg Gatlin, NASA Technical Point of Contact for the contract.

References

[1] Droney, C., Harrison, N., Gatlin, G., "Subsonic Ultra-Green Aircraft Research: Transonic Truss-Braced Wing Technical Maturation", 31st Congress of the International Council of the Aeronautical Sciences, Belo Horizonte, Brazil, September 9-14, 2018.

[2] Droney, C., "How sweet the future of aviation", SUGAR Technical Feature Page, August 2017 https://www.boeing.com/features/innovation-quarterly/aug2017/feature-technical-sugar.page

[3] Droney, C. K., Sclafani, A. J., Harrison, N. A., Grasch, A. D., Beyar, M. D., "NASA/CR-2018-xxxx, Subsonic Ultra Green Aircraft Research: Phase III – Mach 0.75 Transonic Truss-Braced Wing Design", Boeing Research and Technology, Huntington Beach, CA, July 2018.

[4] Harrison, N. A., and Droney, C. K., "NASA/CR –2018- xxxx, Subsonic Ultra Green Aircraft Research: Phase IV, Volume I - Mach 0.80 Transonic Truss-Braced Wing High-Speed Design", Boeing Research and Technology, Huntington Beach, CA, June 2018.

[5] Maldonado, D., Housman, J. A., Duensing, J. C., Jensen, J. C., Kiris, C. C., Viken, S. A., Hunter, C. A., Frink, N. T., McMillin, S. N.: Computational Simulations of a Mach 0.745 Transonic Truss-Braced Wing Design. AIAA SciTech 2020 Forum, AIAA-2020-1649, Orlando, FL, January 6-10, 2020.

[6] Viken, S. A., Hunter, C. A., McMillin, S. N., Gatlin, G. M., Maldonado, D., Housman, J. A., Duensing, J. C., Jensen, J. C., Kiris, C. C, NASA Technical Memorandum, Comparison of Computational Predictions of the Mach 0.80 Transonic Truss-Braced Wing Configuration with Experimental Data, Publication Date TBD.

[7] Menter, F. R., "Two-Equation Eddy-Viscosity Turbulence Models for Engineering Applications," AIAA Journal, Vol. 32, No. 8, August 1994, pp. 1598-1605

[8] Harrison, N. A., Sclafani, A. J., Beyar, M. D., Dickey, E. D., Intravartolo, N. M., "NASA/CR-20xx- xxxx, Subsonic Ultra Green Aircraft Research: Phase IV Final Report, Volume II - Transonic Truss-Braced Wing High-Speed Test Report", Boeing Research and Technology, Huntington Beach, CA, Publication Date TBD.

[9] Kiris, C., Housman, J., Barad, M., Brehm, C., Sozer, E., and Moini-Yekta, S., "Computational Framework for Launch, Ascent, and Vehicle Aerodynamics (LAVA)," Aerospace Science and Technology, Vol. 55, 2016, pp. 189–219.

[10] Vinokur, M., "Conservation Equations of Gasdynamics in Curvilinear Coordinate Systems," Journal of Computational Physics, Vol. 14, 1974, pp. 105–125.

[11] Spalart, S. R., and Allmaras, S. A., "A One-Equation Turbulence Model for Aerodynamic Flows," 30th Aerospace Sciences Meeting and Exhibit, Reno, NV, 1992. AIAA-92-0439.

[12] Shur, M. L., Strelets, M. K., Travin, A. K., and Spalart, P. R.: Turbulence Modeling in Rotating and Curved Channels: "Assessing the Spalart-Shur Correction," AIAA Journal Vol. 38, No. 5, 2000, pp. 784-792.

[13] Spalart, P. R.: "Strategies for Turbulence Modeling and Simulation. International Journal of Heat and Fluid Flow," Vol. 21, 2000, pp. 252-263.

[14] Housman, J., Kiris, C., and Hafez, M., "Time-Derivative Preconditioning Methods for Multicomponent Flows - Part I: Riemann Problems," Journal of Applied Mechanics, Vol. 76, No. 2, 2009.

[15] Housman, J., Kiris, C., and Hafez, M., "Time-Derivative Preconditioning Methods for Multicomponent Flows - Part II: Two-Dimensional Applications," Journal of Applied Mechanics, Vol. 76, No. 3, 2009.

[16] Saad, Youcef, and Martin H. Schultz. "GMRES: A generalized minimal residual algorithm for solving nonsymmetric linear systems." SIAM Journal on scientific and statistical computing, Vol. 7, No. 3, July 1986, pp. 856-869.

[17] Nichols, R. H., Buning, P. G., "User's Manual for OVERFLOW 2.2" Version 2.2, March 2019. https://overflow.larc.nasa.gov/users-manual-for-overflow-2-2/

[18] Menter, F. R., Kuntz, M., and Langtry, R., "Ten Years of Industrial Experience with the SST Turbulence Model," Turbulence, Heat and Mass Transfer 4, ed: K. Hanjalic, Y. Nagano, and M. Tummers, Begell House, Inc., 2003, pp. 625 - 632.

[19] Smirnov, P. E., Menter, F. R., "Sensitization of the SST Turbulence Model to Rotation and Curvature by Applying the Spalart-Shur Correction Term," ASME Journal of Turbomachinery, Vol. 131, October 2009, 041010

[20] Frink, N. T.: "Tetrahedral Unstructured Navier-Stokes Method for Turbulent Flow," AIAA Journal, Vol. 36, No. 11, Nov. 1998, pp. 1975-1982.

[21] Frink, N. T., Pirzadeh, S. Z., Parikh, P. C., Pandya, M. J., and Bhat, M. K.: "The NASA Tetrahedral Unstructured Software System," The Aeronautical Journal, Vol. 104, No. 1040, October 2000, pp. 491-499.
[22] Pandya, M. J., Jespersen, D. C., Diskin, B., Thomas, J. L., Frink, N. T.: Accuracy, Scalability, and Efficiency of Mixed-Element USM3D for Benchmark Three-Dimensional Flows, AIAA SciTech 2019 Forum, AIAA 2019-2333, San Diego, CA, January 7-11, 2019.
[23] Test Requirements Document, SUGAR Phase IV Mach 0.8 Test 11-0367, NASA Ames Unitary Plan Wind Tunnel.
[24] T11-xxxx: Cavity Correction Methodology, Eric Paciano. September 2019, Test No. 11-0343 and Test No. 0367.
[25] Dreere, K. A., Viken, J. K., Viken, S. A., Carter, M. B., Wiese, M. R., and Farr, N., : Computational Analysis of a Wing Designed for the X-57 Distributed Electric Propulsion Aircraft, AIAA Aviation 2017 Forum, AIAA 2017-3923, Denver, CO, June 2, 2017.